ACS APPLIED NANO MATERIALS

www.acsanm.org Article

Controlling Photoluminescence for Optoelectronic Applications via Precision Fabrication of Quantum Dot/Au Nanoparticle Hybrid Assemblies

Anum Nisar, Harini Hapuarachchi, Laurent Lermusiaux, Jared H. Cole,* and Alison M. Funston*

Cite This: *ACS Appl. Nano Mater.* 2022, 5, 3213−3228 Read Online

ACCESS | Metrics & More | Article Recommendations | Supporting Information

Downloaded via MONASH UNIV on June 29, 2022 at 03:04:06 (UTC).
See https://pubs.acs.org/sharingguidelines for options on how to legitimately share published articles.

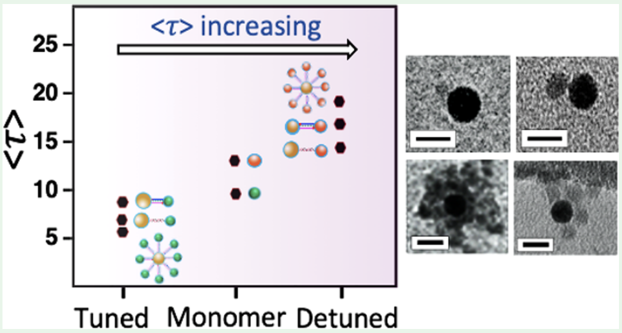

ABSTRACT: The distance-dependent interaction of an emitter with a plasmonic nanoparticle or surface forms the basis for the application of such systems within optoelectronics. Semiconductor quantum dots (QDs) are robust emitters due to their photostability. A key challenge is the formation of well-defined assemblies containing QDs and plasmonic nanoparticles in high purity. Here, we present the translation of DNA-based self-assembly to assemble metal and semiconductor nanocrystals into hybrid structures. The high purity of the assemblies, including dimers and higher-order core−satellite structures, allows fundamental investigation of the plasmon−exciton interaction. In contrast to the increase in the QD emission rate and enhancement in steady-state photoluminescence observed for overlap between the QD emission and localized surface plasmon resonance, significant detuning of these energies leads to lengthening of the QD emission lifetime (reduction of the emission rate) up to 1.7-fold and enhancement in steady-state photoluminescence of 15−75%. These results are understood in terms of the Purcell effect, where the gold nanoparticle acts as a damped, nanoscale cavity. We show that the response is driven by the interference experienced by the emitter for parallel and perpendicular field orientations. This provides a mechanism for control of the emission rate of a QD by a metal nanoparticle and a much wider range of lifetimes than previously understood.

KEYWORDS: *hybrid assemblies, purcell effect, DNA-based self-assembly, quantum dots, plasmonics, plasmon-exciton Interactions*

■ INTRODUCTION

Control of the emission of luminescent species is integral to their application in optoelectronics, including LEDs and photovoltaics. One method to modify the excitonic states of emitters, and thereby increase their emission intensity, is via the use of metal nanoparticle nanocavities. These exploit the Purcell effect by changing the photonic environment (i.e., the dielectric environment) of nearby emitters. Of the exciton−plasmon systems for potential use in LEDs and light harvesting and/or photovoltaics, those containing semiconductor quantum dots (QDs) also offer significant advantages compared to organic fluorophores, including photostability, high quantum yield, high absorption cross-section, and narrow, tunable emission.[1,2] As such, hybrid structures incorporating quantum emitters and metal nanoparticles are promising materials for optoelectronics.

One approach to improve the brightness of LEDs is to increase the emission intensity of the emissive species. Such an increase has been achieved for coupled metal nanoparticle/QD systems (compared to the uncoupled QDs) when the metal and QD spectra are in resonance.[3] The magnitude of the increase is a function of interparticle separation.[4] In contrast to the requirement for LEDs, an increase in absorption cross-section and photoluminescence lifetime are desirable characteristics for photovoltaic systems. The former is also able to be achieved within coupled metal nanoparticle/QD systems due to the presence of metal nanoparticles, which have high absorption cross sections at small sizes. The latter has been observed in the strong coupling regime,[5] with few reports in the more readily achievable weak coupling regime (with the nanoparticles at larger interparticle separation). Additionally, the fundamental photophysics of coupled metal nanoparticle/QD systems where the metal and QD optical properties are very detuned from one another have received little attention.

Metal nanoparticles much smaller than the wavelength of incident light (λ) exhibit strong resonant excitations known as localized surface plasmon resonances (LSPRs).[6,7] These excitations enable metal nanoparticles to act as nanoscale

Received: October 20, 2021
Accepted: February 8, 2022
Published: March 4, 2022

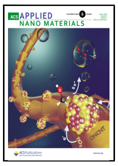

ACS Publications

© 2022 American Chemical Society

https://doi.org/10.1021/acsanm.1c03522

optical cavities able to focus electromagnetic energy to spots much smaller than λ overcoming the half-wavelength size limitation of conventional optical cavities.[8,9] As metal nanoparticles modify the electric field at their surface, they influence the dielectric environment of emitters in close proximity and consequently their emission (intensity and emission rate).[10] A competing, also distance dependent, interaction is damping occurring due to energy transfer from the emitter to the metal particle acceptor. The competition between field enhancement and nonradiative damping controls the optical response.[11] Effective plasmon−fluorophore coupling requires the close proximity of the plasmon and fluorophore and significant overlap of the emission spectrum of the fluorophore with the LSPR of the metal nanocrystals.[11]

Hybrid plasmon-exciton films have been realized using the layer-by-layer approach with layers of Au or QD thin films separated by well-defined spacer layers. Within these, both quenching and enhancement of the PL intensity were achieved upon tuning the spectral overlap and variation of the polymer/polyelectrolyte layers between the films.[12−14] A major concern for NP-based films is the aggregation of NPs upon drying. This causes changes in the LSPR of the metal NP and the emission of the fluorophore, thereby modifying the overall optical response of the hybrid films compared to their counterparts in the solution.[15] Electron beam lithography approaches have also been widely employed to prepare two-dimensional hybrid structures, although gap variation and surface roughness lead to variations in the optical response of the coupled nanoparticles.[16,17]

Colloidal methods have the potential for the development of three-dimensional structures in scalable quantities. Energy transfer in electrostatically assembled clusters containing multiple dyes or quantum dots around metal nanoparticles showed a 2−3-fold reduction in the lifetime of the fluorophore, while the transfer efficiency was able to be modulated from 30% to 55% via a change in the concentration of either gold nanoparticles or the fluorophore.[18,19] However, such approaches do not provide control over the number of emitters or interparticle separation. To overcome this, chemical coupling of the metal and fluorophore with short biological or chemical linkers, or silica encapsulation have been employed to develop hybrid structures,[20−22] although generally, these methods provide only limited control over metal−fluorophore distances and stoichiometry, limiting their use.

Consequently, a key requirement in this field is the development of assembly methods with the ability to fully control the relative location, orientation, and interparticle separation in coupled plasmon-exciton systems. DNA has been exploited to achieve self-assembly of gold nanoparticles by hybridization of single-stranded DNA attached to metal nanoparticles as well as sophisticated DNA origami scaffolds.[23−26] The variable length of the DNA strands offers flexibility in the interparticle separation, and purification techniques enable control over the number of particles in the assembly.[27,28] Alivisatos pioneered the DNA-based self-assembly of gold nanoparticles into discrete structures.[29] Subsequently, improved protocols for DNA-based gold nanoparticle assembly have been developed.[30] In contrast, DNA-based QD assembly protocols are relatively underdeveloped[30−32] with a key enabling capability, that is, the purification of particles with one (or a given number) of attached DNA strands per particle lacking.

Because of the distance dependence of the photophysical processes occurring in metal−fluorophore systems, their optical properties vary between quenching[33,34] and enhancement[35,36] of the photoluminescence intensity of the emitter. Within discrete hybrid assemblies with a good overlap of the metal LSPR and fluorophore emission, strong quenching of the QD PL intensity is observed,[34,37] but at a given separation distance a crossover from quenching to enhancement in the PL intensity occurs.[38−40] A 2.5 to 8-fold photoluminescence enhancement with little to no change in photoluminescence lifetimes for on-resonant Au-QD assemblies with interparticle separations in the range of 2−20 nm have been reported.[41−43] Higher degrees of steady-state photoluminescent enhancement have been observed for QD-Au hybrid films where increases of up to 50-fold have been demonstrated,[44,45] illustrating the potential for these systems to be utilized in LEDs. In contrast, PL decay measurements show a reduction in the lifetime of the emitter close to the metal for all the reported hybrid systems, irrespective of quenching and enhancement in the PL intensity.[17,46]

Here, we report an approach that overcomes many synthetic challenges to allow the controlled organization of quantum emitters near gold nanoparticles. The assemblies are achieved with high colloidal stability, reproducibility, and purity. The hybrid assemblies show increased control over the QD lifetime with an increase in the lifetime observed when the QDs and LSPR of the metal are highly detuned, along with the expected shortening of the lifetime when these are resonant. The photoluminescence consistently shows an increase in intensity. By modeling single metal-QD dimers using an open quantum systems framework, we demonstrate the orientation dependence of their photoluminescence. The origin of PL intensity enhancements observed experimentally in our colloidal ensembles can be attributed to the dominance of axial field enhancements.

■ RESULTS AND DISCUSSION

In this work, we synthesize discrete assemblies of AuNPs and CdSe/CdS QDs using a DNA-driven self-assembly approach, and characterize and theoretically model their optical response. Assemblies are formed by mixing two sets of particles functionalized with complementary single-stranded DNA as shown in Scheme 1. The desired assemblies are made of gold nanospheres (10 nm diameter, AuNS_{10}) or nanorods surrounded by one (hybrid dimers) or several QDs (core−satellite). To obtain the hybrid nanostructures in high yield, an electrophoretic method to obtain QDs attached to exactly one DNA strand per particle was used, while retaining the fluorescence quantum yield, is developed. This ability expands the currently available library of assembled nanostructures able to be achieved with the possibility for the selective incorporation of semiconductor materials into already established DNA-based structures.

The number of QDs attached to the gold core is controlled by varying the number of DNA strands adsorbed onto the AuNPs. The distance between the AuNPs and QDs is given by the DNA length. Two different sets of DNA strands which are 34 and 100 bases long (theoretical distances of 10 and 34 nm) are used, as is a final purification step, again with electrophoresis, to obtain the desired products in high purity. Overall, this DNA-based electrophoretic approach allows control over the number of emitters in the hybrid assembly, the interparticle

Scheme 1. Formation of Hybrid Structures with Different Strand Lengths of DNA[a]

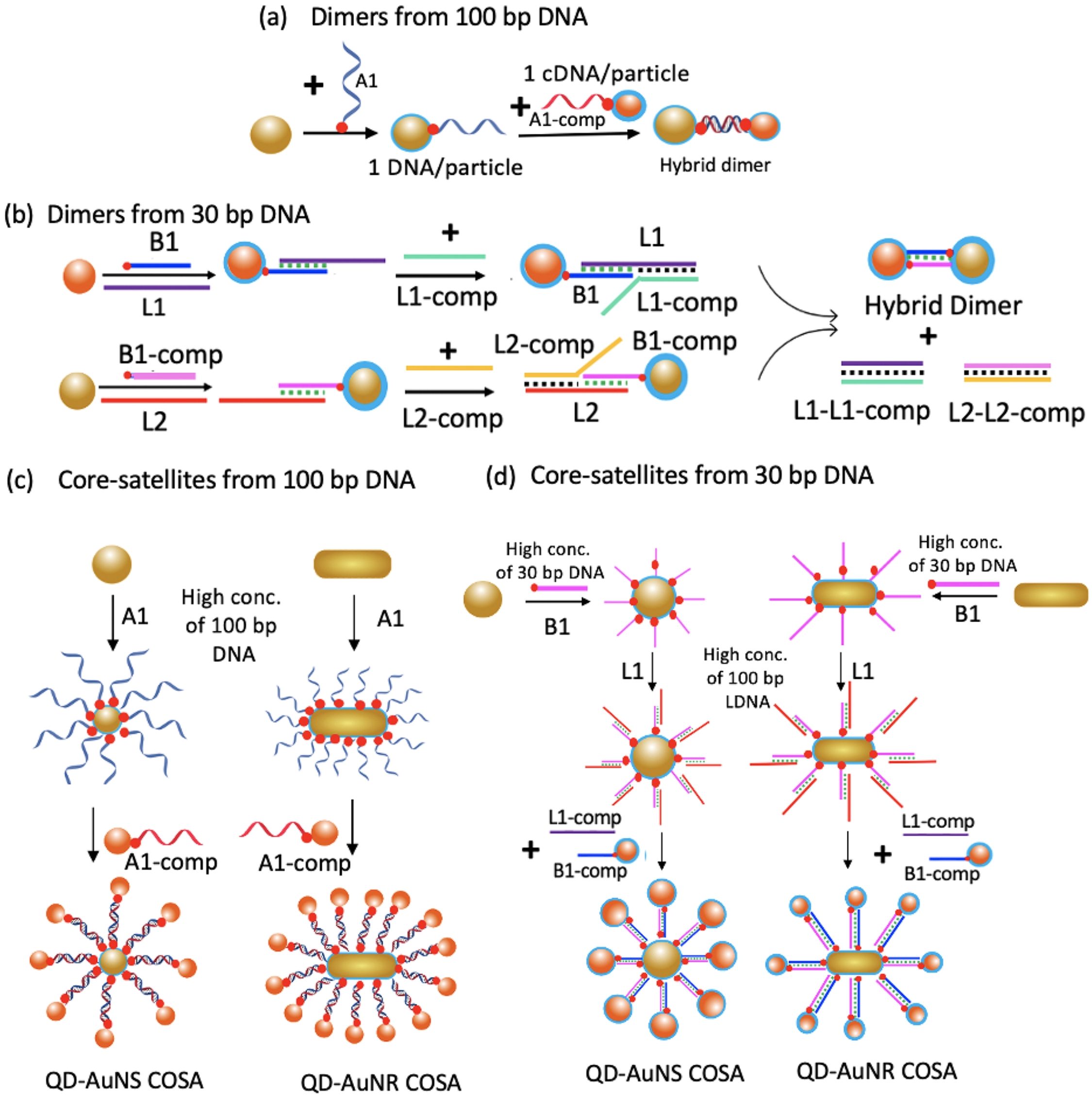

[a]The wiggly lines and straight lines represent 100 and 30 bp DNA, respectively. The orange sphere represents a quantum dot while the golden sphere and rod are representing gold nanosphere and nanorod. (a) Hybrid dimers with long DNA (100 bp), ~34 nm interparticle separation. (b) Hybrid dimers with short DNA (30 bp), ~10 nm interparticle separation. (c) Hybrid COSA with long DNA (100 bp), ~34 nm interparticle separation. (d) Hybrid COSA with short DNA (30 bp), ~10 nm interparticle separation.

separation between AuNP and QDs, and the nanoparticle size and shape.

Building Blocks for Self-Assembly. The transferable nature of the DNA functionalization across different-sized nanoparticles of the same material (and therefore with the same surface chemistry[32]) allows the incorporation of quantum dots of different sizes and therefore different energy band gaps into the assemblies using the same protocols. The QDs used have diameters of 3.5 ± 1.3 nm (Q550), 4.5 ± 0.8 nm (Q570), 6.0 ± 0.6 nm (Q610), and 8.0 ± 1.0 nm (Q650) with the wavelength of their lowest energy absorption 545 nm (Q550), 548 nm (Q570), 589 nm (Q610), and 622 nm (Q650). The gold nanospheres have a diameter of 10.0 ± 0.7 nm.

The metal nanoparticles and quantum dots are synthesized according to standard protocols[47−49] and electron microscopy images, along with size distribution histograms, of the nanoparticles are shown in Figure S1. The synthesis of quantum dots was carried out using organic solvents, which are known to form a colloid with higher monodispersity and quantum yield for CdSe QDs than aqueous syntheses. The former is required to achieve well-separated, discrete bands on the agarose gel employed in the DNA-based assembly approach, while the latter is required for visualization of the separated particles. Phase transfer of the QDs into an aqueous solution is achieved with PsAA allowing good retention of the QD PL. Metal nanoparticles are ligand exchanged with *bis*(*p*-sulfonatophenyl)phenylphosphine (BSPP). We refer to the gold nanospheres as AuNS_{10} and gold nanorods as $\mathrm{AuNR}_{2.7}$.

Functionalization of QDs and Au Nanoparticles with DNA. To enable the formation of the desired discrete assemblies in high purity, QDs and gold nanoparticles attached to single complementary DNA strands are prepared and mixed as shown in Scheme 1.

To perform DNA functionalization of the QDs with 100-mer ssDNA, a concentrated solution of ligand-exchanged QDs (~25 μM) were incubated with 100 bp A1-comp trithiolated

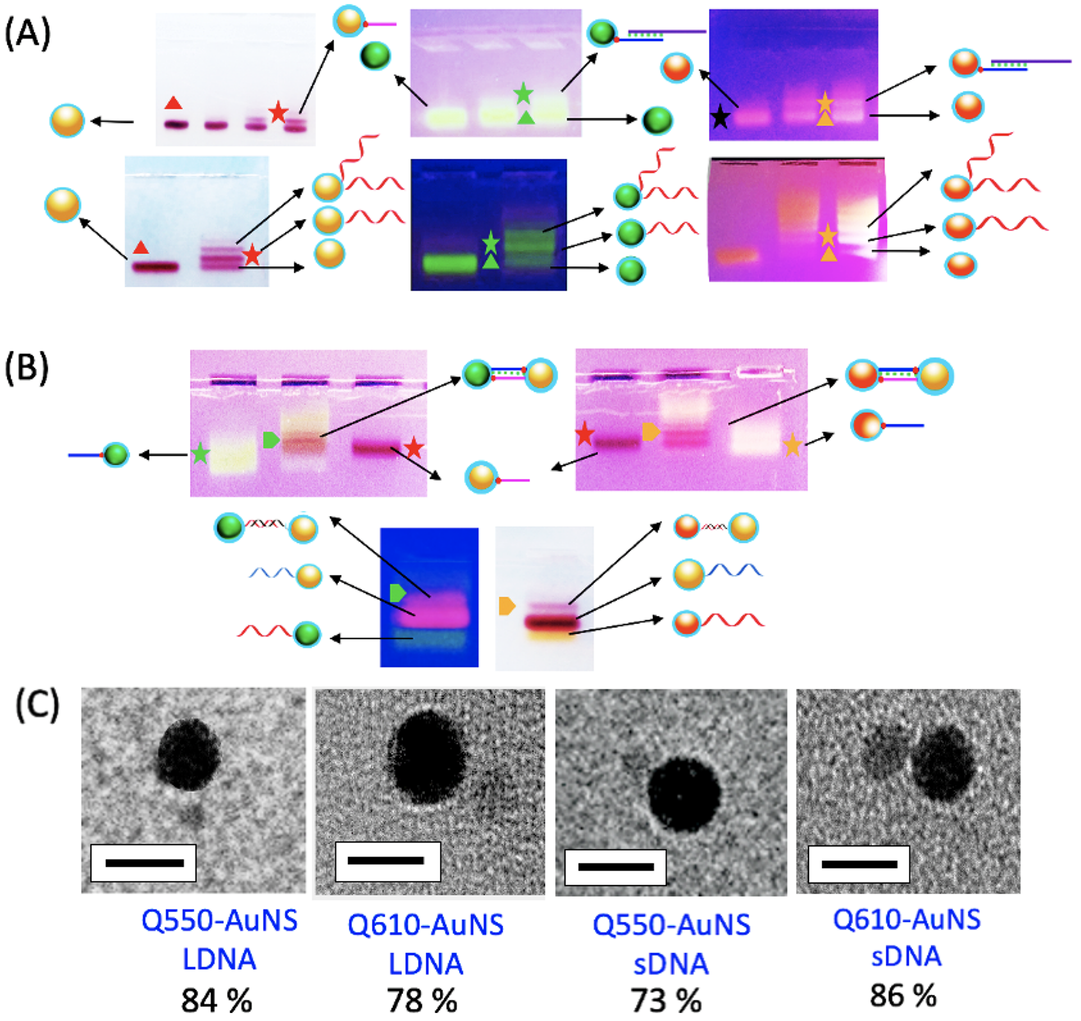

Figure 1. (A) Gel images showing the purification of $AuNS_{10}$, Q550, and Q610 with defined numbers of DNA strands per particle using agarose gel of 2.75%, 4.1%, and 3.4%, respectively, for 35−40 min at 80 V. The $AuNS_{10}$, Q550, and Q610 are represented as golden-, green-, and orange-colored spheres, respectively. The curved and straight lines indicate the attachment of long DNA (LDNA) and short DNA (sDNA), respectively. The DNA concentration increases from left to right in the gel figures. The fastest band contains nanocrystals with no DNA; AuNS (red triangle), Q550 (green triangle), and Q610 (orange triangle). The second band is nanocrystals with 1 DNA/particle, that is, $AuNS_{10}$-1DNA (red star), Q550-1DNA (green star), and Q610-1DNA (orange star). (B) Purification of the hybrid Q550-$AuNS_{10}$ (green diamond) and Q610-$AuNS_{10}$ dimer assemblies (orange diamond) from the unconjugated $AuNS_{10}$-1DNA (red star) and Q550-1DNA (green star) and Q610-1DNA (orange star) particles after running on 2.5% agarose gel at 80 V for 30 min. (C) Representative TEM images of the hybrid Q550-$AuNS_{10}$ and Q610-$AuNS_{10}$ dimers synthesized with 30 and 100 bp of DNA. Scale bar is 10 nm

DNA strands, at a concentration optimized for attachment of one strand of DNA per particle (∼10−40 μM for QDs), generally close to a 1:1 ratio of QD/DNA, in salt for 24 h to allow adsorption of the thiol groups to the nanoparticle surface. The concentration of the QDs used here is higher than that of the gold nanoparticles to allow their visualization in the gel, however, the relative ratio of DNA to nanoparticles required for the QDs is lower compared to that for the gold nanoparticles. The presence of salt reduces the electrostatic repulsion between the particle and DNA strands, allowing the DNA to bind to the nanoparticle surface.[50] Following this, to improve the colloidal stability and photoluminescence quantum yield, QDs were passivated with mercapto(ethylene glycol)$_6$ carboxylate. PEGylation also promotes the dispersion of QDs in the high salt-containing buffer media required for both electrophoresis and DNA hybridization. The resultant nanoparticle surfaces are densely covered with PEG and BSPP.[51]

Electrophoretic separation of QDs attached to different numbers of DNA strands is carried out by optimization of the salt concentration and gel density, using different DNA concentrations (Figure 1A). Well-separated, clear bands were observed upon electrophoretic separation of the DNA-functionalized QDs, indicating separation of samples containing discrete numbers of DNA strands per particle. The number of DNA strands attached to the nanoparticles is determined by a comparison of each band position with respect to the reference band of the nanoparticles without DNA. An increase in DNA concentration leads to the monomer band (without DNA) disappearing, along with the appearance of higher bands indicative of QDs with multiple DNA strands per particle, including one, two, and three strands/particle. The agarose gel concentration ranges from 3.2−4.1% depending on the size of the QDs. This is relatively high compared to that used for gold nanoparticles (2.75%) due to the small size of the QDs compared to the gold nanoparticles. The DNA-functionalized

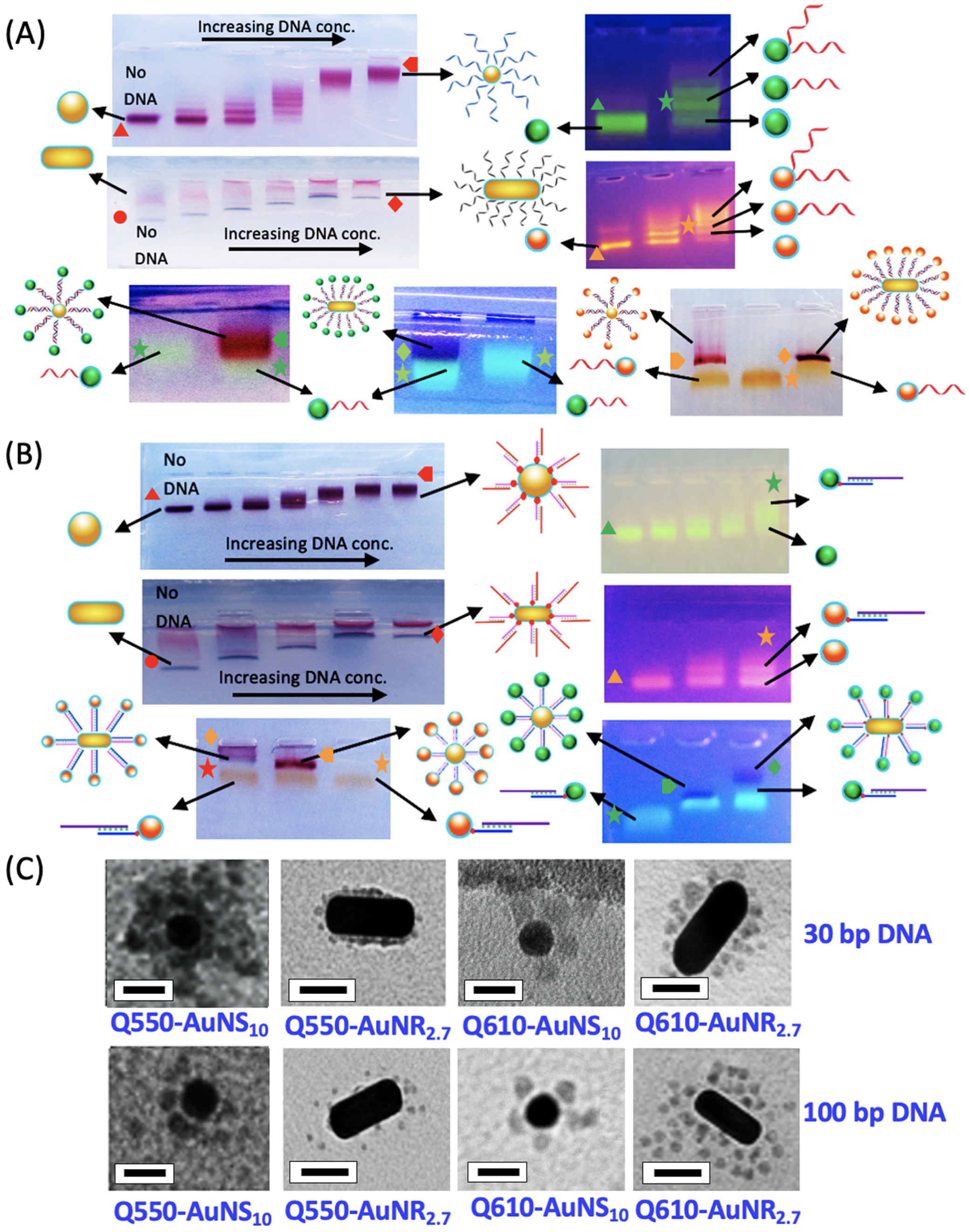

Figure 2. Formation and purification of hybrid core−satellite assemblies with (A) long DNA (LDNA) of 100 bp (curved lines) and (B) short DNA (sDNA) of 30 bp (straight lines). The DNA concentration increases from left to right with the leftmost band the particle with no added DNA. Gel images show the DNA purification of fully functionalized central AuNS$_{10}$ (red pointer) and AuNR$_{2.7}$ (red diamond) with reference to the particle with no attached DNA; AuNS$_{10}$ (red triangle) and AuNR$_{2.7}$ (red circle) on 1% agarose gel at 80 V for 35 min. Hybrid Q550-AuNS$_{10}$ COSA (green pointer) and Q610-AuNS$_{10}$ COSA (orange pointer) assemblies were purified from the unconjugated Q550-1-DNA (green star) and Q610-1DNA (orange star) particles by running on 1.5% agarose gel at 80 V for 30 min. (C) TEM characterization of the synthesized hybrid COSA assemblies of Q550 and Q610 with 30 and 100 bp DNA. The scale bar is 20 nm.

QDs were bright enough to be visualized in the gel from their luminescence (Figure 1A) due to the relatively good retention of their quantum yield without the use of staining agents such as ethidium bromide. Extraction of particles functionalized with one DNA strand per particle was achieved by slicing out the separated band and soaking the gel slice in TBE buffer overnight.

To form assemblies with short DNA strands to realize stronger interaction between the Au and QD, the challenge is to achieve well-resolved gel bands containing one DNA strand per particle on purification via electrophoresis. The short-chain length of the 30 bp DNA does not allow a significant size increase of the DNA−nanoparticle conjugate (compared to the nanoparticle itself), which makes it difficult to purify via electrophoresis. A toehold-mediated DNA displacement approach was thus used to achieve this goal[50] as outlined in Scheme 1B. Different volumes of 30 bp B1 DNA (100 μM) are added to a concentrated solution of the QDs, along with an equimolar concentration of the 100 bp long nonfunctionalized lengthening DNA strand (L1). The L1 DNA has 15 bp

Table 1. Photophysics of the Hybrid Assemblies Fabricated Using 30 bp DNA Linkers

assembly type	NP 1	NP 2	# NP 2	J ($\times 10^{-12}$ cm^6 mmol^{-1})	$\langle\tau\rangle$ (ns) QD-ref	$\langle\tau\rangle$ (ns) assembly
dimer	$AuNS_{10}$	Q550	1	4.78	9.9 ± 0.7	7.8 ± 0.4
dimer	$AuNS_{10}$	Q610	1	2.78	12.9 ± 0.4	16.3 ± 0.3
COSA	$AuNS_{10}$	Q550	9 ± 2	4.78	8.4 ± 0.4	6.5 ± 0.4
COSA	$AuNS_{10}$	Q570	7 ± 2	3.89	13.1 ± 0.4	14.4 ± 0.3
COSA	$AuNS_{10}$	Q610	5 ± 2	2.78	12.0 ± 0.3	19.8 ± 0.5
COSA	$AuNS_{10}$	Q650	5 ± 2	1.62	9.0 ± 0.4	9.7 ± 0.4
COSA	$AuNR_{2.7}$	Q550	18 ± 4	1.61	8.4 ± 0.4	6.7 ± 0.4
COSA	$AuNR_{2.7}$	Q570	16 ± 4	2.80	13.1 ± 0.4	16.0 ± 0.6
COSA	$AuNR_{2.7}$	Q610	13 ± 4	2.88	12.0 ± 0.3	20.3 ± 0.5
COSA	$AuNR_{2.7}$	Q650	13 ± 4	3.93	9.0 ± 0.4	10.7 ± 0.3

complementary to the B1 DNA. The B1 DNA attaches the AuNP via trithiol moiety while its overhanging strand hybridizes with the L1 DNA. This conjugation increases the effective length/bulk of the DNA, therefore facilitating the separation of the nanoparticles in the gel (Figure 1A).[50]

The DNA functionalization and separation of products to isolate nanoparticles containing one DNA strand per particle of small gold nanospheres (D = 10 nm) is well known and was carried out according to literature procedures[32,52−54] by incubating gold nanoparticles (~1−5 μM) with 100 bp A1 DNA (~5−30 μM) and their subsequent purification via gel electrophoresis (shown in Figure 1A). The procedure outlined above was repeated for 30 bp DNA with gold nanoparticles to achieve one strand of B1-comp and L2 DNA per gold nanoparticle.[50] The nanoparticles were then used for the formation of the assemblies.

Self-Assembly of Au-QD Dimers. To form discrete QD/Au hybrid dimers in high yield with the 100 bp DNA linker (Scheme 1A), the AuNP and QDs (containing one A1-DNA and one complementary A1-DNA per particle, respectively) are incubated in the presence of salt (Scheme 1A). Hybrid Au-QD dimer assemblies with 30 bp linkers are formed by mixing B1 and L1 DNA functionalized QDs with B1-comp and L2 DNA functionalized gold nanoparticles along with L1-comp and L2-comp lengthening DNA strands. These were hybridized overnight, resulting in a branch migration which displaces the stable final duplex (consisting of the nonthiolated 100-mer DNA pairs of L1−L1-comp, L2−L2-comp), along with the short DNA bound Au-QD assembly.

Following incubation of the DNA functionalized nanoparticles, the assemblies were further purified via electrophoresis to remove unhybridized nanoparticles and higher-order assemblies. Figure 1B presents the gels (2.5%) of the electrophoretic purification of the short and long DNA assembled hybrid dimers Q550-$AuNS_{10}$ and Q610-$AuNS_{10}$. The first and second bands (from the bottom) in the gels correspond to the monomer QD/AuNPs functionalized with one DNA strand, respectively, while the third band corresponds to the hybrid dimer assembly. No slower bands, indicative of the formation of higher-order assemblies, are observed. The bands containing the assemblies were eluted from the gel and characterized by transmission electron microscopy (TEM) as shown in Figure 1C. The high contrast particles in the TEM images are gold nanoparticles, while the nanoparticles with lower contrast are the semiconductor QDs. The dimer purity ranges from 73% to 86% (Figure S4, Figure S5) following deposition on the substrate. The distance between the Au nanoparticle and QD when deposited on a substrate, as measured from the TEM images, is 1.0−1.5 nm with 100 bp DNA and 0.5−1.0 nm with 30 bp DNA. The smaller interparticle separation upon deposition compared to that expected based on the length of the DNA double-stranded helix linker is likely due to the drying effects upon deposition, including van der Waals interactions between the particles and capillary drying effects. For DNA-linked assemblies in solution at low salt concentrations, electrostatic repulsion between the negatively charged nanoparticle surfaces and DNA backbone result in increased rigidity, and even slight stretching, of the DNA scaffold such that the DNA is fully extended.[51,55] At higher salt concentration, these charges are shielded and the interparticle separation can be significantly shorter.[51] The salt concentration used here is low, and so the average DNA linker length between the metal NP and QD with fully extended 30 bp and 100 bp DNA are ~10 and ~34 nm, respectively with the distribution of lengths within a standard deviation of the order of 3 nm.[51] The intrinsic polydispersity of the colloidal nanoparticle samples (Figure S1, Table S1) convolves with the distribution in linker lengths, resulting in a distribution of center-to-center distances of (for the worst case here, Q550 hybrids) a standard deviation of center-to-center distances of ~3.1 nm (center-to-center distance of ~13.5 nm of the Q550 QDs linked by 30 bp DNA).

Self-Assembly of Au-QD Core−Satellite (COSA) Structures. The versatility of the DNA-based approach following isolation of QDs containing one DNA strand per particle is highlighted by the adaptation of the DNA hybridization scheme to form Au-QD core−satellite structures. The fabrication of core−satellite hybrid structures (Scheme 1C) containing a metal core and multiple monofunctionalized QD satellites were formed by initially conjugating the central gold nanoparticle with an excess of DNA prior to the self-assembly. The higher DNA density is achieved by mixing the particles with higher DNA (40−90 μM) and salt concentrations (50−100 μM) and is confirmed by lower electrophoretic mobility of the particles on the agarose gel (Figure 2A). The high salt concentration reduces the electrostatic interaction between the negatively charged ssDNA and thus allows a higher DNA density to be functionalized onto the AuNP surface. Additionally, running the cores on the gel separates the DNA-coated particles from excess (nonbinding) DNA strands and is a necessary step prior to assembly. It also has the benefit of purifying the desired nanoparticles from side-products (different shapes, for example) as can be seen in the gel images for the purification of AuNR, which are separated from nanosphere byproducts, the blue and red bands, respectively, in the gels in Figure 2A (~50 nm $AuNS_{50}$).

To form hybrid QD-$AuNS_{10}$ COSA and QD-$AuNR_{2.7}$ COSA assemblies with 100 bp DNA, the fully A1 DNA functionalized $AuNS_{10}$ and $AuNR_{2.7}$ core particles are hybridized with QD satellite particles containing one complementary A1-comp DNA strand per particle. The hybrid core−satellite assemblies were again purified via a second gel electrophoresis step on a diluted gel (1.5%) to separate the hybrid COSA assemblies from the unbound satellites (Figures 2B and S9). The low mobility of the COSA assembly compared to single unconjugated nanoparticles results in separate bands for these species as shown in Figure 2A (lower panel). Similarly, to form 30 bp DNA-based COSA structures a high concentration (40−90 μM) of B1-DNA and L1 lengthening strand are mixed with the core AuNP, which after purification is hybridized with QDs functionalized with one complementary B1-comp and L1-comp DNA duplex per particle as outlined in (Scheme 1D).

The TEM images of the COSA structures in Figures 2C and S3 show the distribution of the number of satellites per metal core ranges from 1−10 for $AuNS_{10}$ and 1−20 for $AuNR_{2.7}$ hybrid assemblies (Figure S4, Table 1). As expected, the number of satellites around the metal core increases as the size of the QD increases from Q550 to Q650. The coverage of the satellites around the core NP also depends upon the available surface area of the core NP. Therefore, a higher DNA valency, and therefore a higher number of QD satellites, is observed for gold nanorod cores $AuNR_{2.7}$ relative to gold nanospheres of 10 nm diameter. For core−satellite assemblies, the distribution of the QDs around the gold core nanoparticle most frequently appear to be clustered together (Figure 2C). This is attributed to capillary forces upon drying and, in solution, it is likely the satellites are not clustered and more evenly distributed around the core.

Photochemistry. The 1:1 metal/QD assemblies allow the effect of the presence of just one metal nanoparticle on a QD to be quantified, and the experimentally observed optical response accurately modeled to understand the fundamental theoretical basis of the observed photophysics.

The series of QD sizes incorporated into the assemblies facilitates comparison of the response as a function of the spectral overlap between the gold nanoparticle LSPR energy and emission of the QDs, as shown in Figure S2. There is a higher degree of spectral overlap between Q550 and the gold nanospheres ($AuNS_{10}$) relative to these with Q570, Q610 and Q650 ($4.78 > 3.89 > 2.78 > 1.62 \times 10^{-12}$ $cm^6 mmol^{-1}$) respectively. The time-resolved photoluminescence decay for the control samples (before and after DNA functionalization and PEGylation) are presented in Figure S6 and Table S2.

Hybrid Dimers. The emission spectra of the Q550-$AuNS_{10}$ dimers with 30 bp DNA are shown in Figure 3C. The photoluminescence intensity in the Q550-$AuNS_{10}$ dimer increases by 19% compared to the monomer (Figure 3A) before hybridization (24% for the 100 bp dimer (Figure S7A)). The observed enhancement is a consequence of the balance between the enhancement of the electric field and quenching of the QD PL, both of which are distance-dependent, at 10 and 34 nm from the metal particle.[42,56]

The PL decays were fit using a triexponential model, reflecting the broad distribution of emission rates of the QD, and are tabulated in Tables 1 and S3 for dimers linked by 30 bp DNA linkers and Table S4 for 100 bp DNA linkers. The decay histogram for Q550-$AuNS_{10}$ (30 bp DNA linker) is shown in Figure 4A. The average lifetime of Q550 is reduced from that of the reference QD, 9.9 ns, to 7.8 ns upon incorporation of the QD into the dimer (Table 1), a reduction of (7.8 ns/9.9 ns) = 0.79. The increase in the steady-state emission intensity (Figure 3C) and decrease in lifetime for Q550-$AuNS_{10}$ is consistent with literature reports[45,57−59] and attributed to coupling of the QD excited state to the AuNP LSPR.[60] The reduction in the degree of quenching of the lifetime of the 100 bp DNA-based Q550-$AuNS_{10}$ hybrid dimer (7.1 ns/8.7 ns) = 0.82 (Figure S7C, Table S4) compared with that of the shorter linker, along with the greater enhancement in the steady-state PL intensity for this larger separation between the QD and gold nanosphere, is also consistent with literature reports.[57]

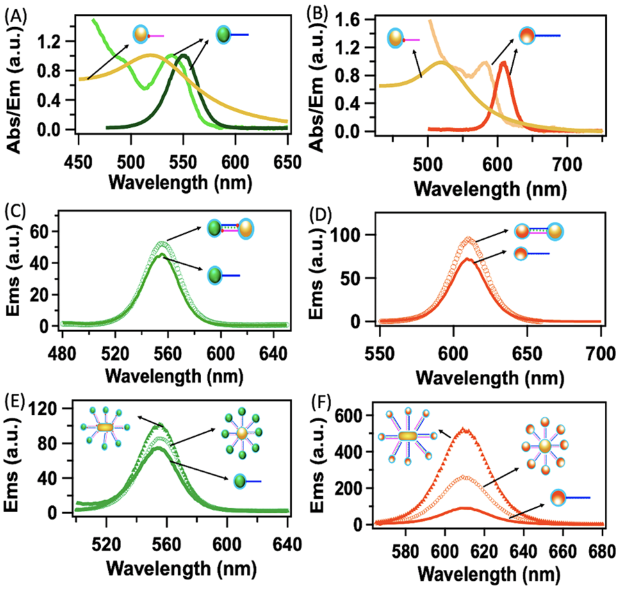

Figure 3. Absorption and emission spectrum of QD overlapped with the extinction spectrum of metal nanoparticle. (A) Q550 (light and dark green) and $AuNS_{10}$ (dark brown). (B) Q610 (light and dark orange) and $AuNS_{10}$ (brown). Steady-state PL measurements of the hybrid assemblies developed by 30 bp DNA (~10 nm interparticle separation). (C) Q550-ref (solid line green) and Q550-$AuNS_{10}$ dimers (circle) at 2 μM concentration. (D) Q610-ref (plain orange) and Q610-$AuNS_{10}$ dimers (circle orange) at 2 μM concentration. (E) Q550-ref (plain green), Q550-$AuNS_{10}$ COSA (green circle) and Q550-$AuNR_{2.7}$ COSA (green triangle) at 3 μM QD concentration. The average number of satellites are 9 ± 2 for Q550-$AuNS_{10}$ and 18 ± 4 for Q550-$AuNR_{2.7}$ COSA assemblies. (F) Q610-ref (plain orange), Q610-$AuNS_{10}$ COSA (circle orange) and Q610-$AuNR_{2.7}$ COSA (triangle orange) assemblies at 3 μM QD concentration. The average number of satellites are 5 ± 2 for Q610-$AuNS_{10}$ and 13 ± 4 for Q610-$AuNR_{2.7}$ COSA assemblies.

In contrast to the results for the Q550 dimer, those for Q610-$AuNS_{10}$ within which the LSPR and QD emission have little spectral overlap (Figure 3B) show an increase in both the steady-state PL intensity and the PL lifetime of the QD, that is, the photoluminescence lifetime of the QD is not quenched but extended (a decrease in the emission rate). The steady-state photoluminescence intensity of Q610-$AuNS_{10}$ dimer linked with a 30 bp DNA linker increases by 23% compared to the reference (Figure 3D), a slightly larger enhancement compared to that for Q550-$AuNS_{10}$. A lengthening of the QD lifetime from $\langle\tau\rangle = 12.9$ ns to $\langle\tau\rangle = 16.4$ ns upon incorporation of the QD into the dimer (30 bp linker length), equating to an increase of (16.4 ns/12.9 ns) = 1.3 is apparent (Figure 4B). For Q610-$AuNS_{10}$ assemblies linked via a 100 bp DNA linker, steady-state PL intensities increased by 13% (Figure S7B), and the PL lifetime increased by 1.2 (Figure S7D) relative to the

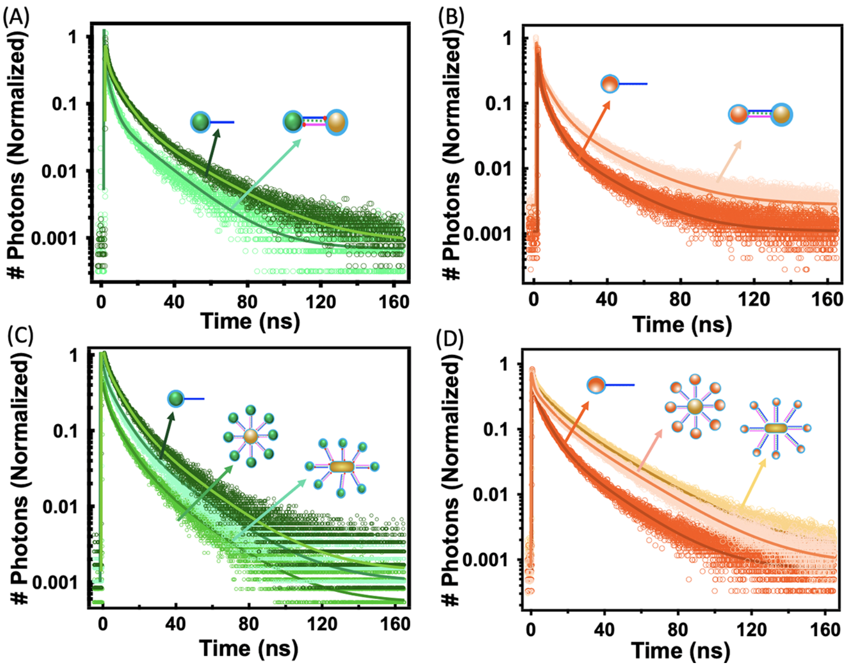

Figure 4. Normalized fluorescence lifetime decays of an ensemble of hybrid assemblies with 30 base pair DNA (∼10 nm interparicle separation) at 425 nm excitation. (A) Q550-ref (dark green) and Q550-AuNS$_{10}$ dimers (light green). (B) Q610-ref (dark orange) and Q610-AuNS$_{10}$ dimers (light orange). (C) Q550-ref (dark green), Q550-AuNS$_{10}$ (medium green) and Q550-AuNR$_{2.7}$ (light green) COSA assemblies. (D) Q610-ref (dark orange) and Q610-AuNS$_{10}$ (light orange) and Q610-AuNR$_{2.7}$ (medium orange) COSA.

reference. Hence, also in contrast to those for the Q550-AuNS$_{10}$ dimer, the changes in PL intensity and lifetime are both more pronounced for the shorter interparticle separation. Comparison of the assembly with the reference (a QD attached to a single strand of DNA) shows that the lifetime lengthening is not due to a change in the surface chemistry upon conjugation with DNA. Insight into the physical origin of the emission enhancement and rate is outlined in the theoretical section below.

The reduction of lifetimes at one end of the spectral overlap scale (i.e., high spectral overlap), combined with the increase in the lifetime for low spectral overlap provides the opportunity for full control of the emission decay rate of the QD in metal−semiconductor hybrid systems. The level of control extends across a time period greater than previously appreciated as a consequence of the increase in the lifetime when the spectral overlap between the nanoparticles is detuned. For all systems, irrespective of the change in emission rate, an increase in the steady-state photoluminescence intensity was observed, although the relative trends with respect to their interparticle separation are different due to the competing factors.

Hybrid Core−Satellite Assemblies. The core−satellite assemblies contain multiple QD particles around a metal nanoparticle, correlating with many donor/single acceptor systems in the framework of energy transfer systems. Relatively little change in the degree of enhancement of the steady-state PL intensity (increase by 29%, Figure 3E)) or lifetime quenching (0.79, Table 1) is observed upon increasing the number of QDs around Q550-AuNS$_{10}$-COSA with 30 bp linking DNA (Figure 2C) compared to the dimer.

Hybrid Q610-AuNS$_{10}$ COSA assemblies with 30 bp linker length, however, have a greater degree of enhancement in the PL intensity (48% enhancement), shown in Figure 3F, compared to the dimer assembly. Similarly, multiple Q610 quantum dots around a single gold nanoparticle also results in a large increase, (19.8 ns/12.0 ns) = 1.65, in the PL lifetime relative to the monomer (Figure 3F, Table 1), and 1.2 relative to the dimer. Enhancement in PL intensity and lengthening of the average lifetime for hybrid assemblies incorporating Q570 and Q650, which have varying degrees of detuning of their emission with the LSPR of AuNS$_{10}$ and 30 bp linkers, is also observed (Figure S10). The degree of spectral overlap for the Q650 hybrid assembly is lower than Q610. A lower enhancement in the magnitude of PL intensity and average lifetime for the Q650 than Q610 hybrid assemblies is however observed. This is attributed to an increase in the center to center spacing between the AuNP and Q650 owing to the bigger size of Q650 with potentially some effect from the low quantum yield of Q650. The quenching of the quantum emitter lifetime is more pronounced for the QD with a higher spectral overlap with AuNS$_{10}$, Q550-AuNS$_{10}$-COSA, for which the quenching dominates the optical response at short interparticle separations. For all other assemblies, a trade-off exists between the degree of spectral overlap and interparticle separation.

Consistent with the results for dimers, increasing the interparticle separation within the core−satellite structures based on AuNS$_{10}$ led to an increase in the steady-state photoluminescence intensity to 31% and 35% for Q550-AuNS$_{10}$-COSA and Q610-AuNS$_{10}$-COSA assemblies, respectively. The lifetime decreased by ∼1 ns for Q550-AuNS$_{10}$-COSA and increased by ∼1 ns for Q610-AuNS$_{10}$-COSA assemblies (Figure S8, Table S5). Control of the assembly structure thus allows tuning of the degree of photoluminescence enhancement and emission rate.

The enhancement effect in the PL intensity and the change in the lifetime values in the hybrid assemblies are more pronounced upon the incorporation of larger, asymmetric plasmonic particles such as gold nanorods. For nanorod

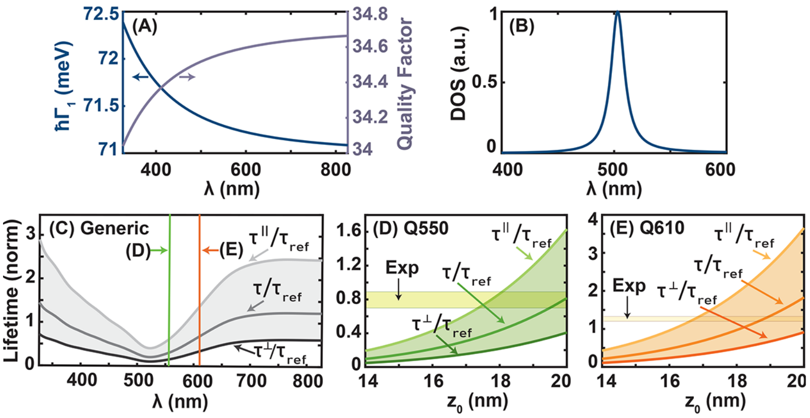

Figure 5. (A) Estimated cavity decay rate, quality factor, and (B) qualitative variation of the density of states for the dipolar ($n = 1$) mode of an r_m ~ 5 nm gold nanoparticle submerged in water. (C) Estimated lifetimes for a generic emitter near a metal nanoparticle calculated using eqs 6a, 6b, and 7. Panels D and E depict cross sections of panel C plotted against the interparticle center separation z_0 at $\lambda = 556$ nm (emission maximum of Q550) and $\lambda = 610$ nm (emission maximum of Q610), respectively.

assemblies with 30 bp DNA linkers, the PL intensity increased from the reference PL values to 45% for Q550-AuNR$_{2.7}$-COSA assemblies and 75% for Q610-AuNR$_{2.7}$-COSA assemblies (Figure 3E,F). The lifetime of Q550 decreased by (6.73 ns/8.44 ns) = 0.80 in Q550-AuNR$_{2.7}$-COSA assemblies and increased by (20.4 ns/12.0 ns) = 1.6 for Q610-AuNR$_{2.7}$-COSA assemblies (Figure 4C,D). With 100 bp DNA linkers, the same assemblies showed an increase in the intensity of the PL, although not to the same degree as observed for the shorter linkers with the lifetime for the Q550-AuNR$_{2.7}$-COSA assembly showing a similar decrease and a smaller increase in the lifetime for Q610-AuNR$_{2.7}$-COSA (Figure S8). The photophysical properties of the AuNR$_{2.7}$-COSA are thus consistent with both AuNS$_{10}$-COSA and hybrid dimers assemblies, although of a greater magnitude. This is presumably due to the strong localization of the near-field of the nanorod at the tips. The same general trends were observed for nanorods of different aspect ratios, with some dependence on nanorod width, as outlined in Figure S11 and Tables S6 and S7 of Supporting Information.

Previous literature shows that the local refractive index of the metal nanoparticle has a large impact on the decay kinetics of QDs in metal−semiconductor assemblies.[61] In the next section, we model the optical properties of these systems to fully understand their origin.

Theoretical Insights. *Impact of the Local Electromagnetic Environment on Spontaneous Emission.* The transition rate (or the transition probability per unit time) of a quantum emitter from an excited state $|e\rangle$ to a ground state $|g\rangle$ follows the Fermi's golden rule given by[62]

$$\gamma_{e\to g} = \frac{2\pi}{\hbar^2}|M_{eg}|^2 g(\omega) \tag{1}$$

The density of states $g(\omega)$ of the electromagnetic environment of the emitter is defined such that $g(\omega)d\omega$ is the number of photon states per unit volume that fall within the angular frequency range ω to $\omega + d\omega$.[62,63] The transition matrix element M_{eg} is obtained as

$$M_{eg} = \langle e|\hat{H}'|g\rangle = -\boldsymbol{\mu}_{eg} . \boldsymbol{\mathcal{E}} \tag{2}$$

where $\hat{H}'$ is the perturbation Hamiltonian caused by light, $\boldsymbol{\mu}_{eg}$ is the electric dipole moment of the transition, and $\boldsymbol{\mathcal{E}}$ is the electric field amplitude experienced by the quantum emitter. It is evident that the transition rate is determined by the interplay between the electric field experienced by the emitter and the density of states.

Damped Nanoscale Cavity Analogy for Gold Nanoparticles. A cavity analogy can be used to describe how an MNP placed in nanoscale proximity alters the electromagnetic environment of a coupled QD. The total cavity decay rate Γ_n (should not be confused with the emitter decay rate γ), the quality factor Q_n and the effective mode volume V_n of the nth cavity-like plasmonic mode of a spherical metal nanoparticle with radius r_m can be estimated using the Drude approximation as $\Gamma_n = \Gamma_{abs} + \Gamma_n^{rad}$ and $Q_n = \omega_n/\Gamma_n$ where[61]

$$\Gamma_n^{rad} = \frac{(2n+1)\epsilon_b}{n\epsilon_\infty + (n+1)\epsilon_b}\omega_n\frac{(n+1)(k_b r_m)^{2n+1}}{n(2n-1)!!(2n+1)!!} \tag{3}$$

$$\omega_n = \omega_p\sqrt{n/[n\epsilon_\infty + (n+1)\epsilon_b]} \tag{4}$$

$$V_n = \frac{n\epsilon_\infty + (n+1)\epsilon_b}{(2n+1)\epsilon_b}\frac{9}{(2n+1)(n+1)}\frac{4}{3}\pi r_m^3 \tag{5}$$

In the above equations, ω_p and Γ_{abs} represent the bulk plasma frequency and the ohmic loss rate of the metal, Γ_n^{rad} is the radiative scattering rate, ϵ_b is the relative permittivity of the nonmagnetic submerging medium (where $n_b = \sqrt{\epsilon_b}$ is the background refractive index), ϵ_∞ is the contribution of bound electrons in the metal dielectric constant and $k_b = n_b k = 2\pi n_b/\lambda$ is the wavenumber in the background medium for free space wavelength λ (and free space wavenumber k).

A dipole ($n = 1$) mode volume V_1 ~ 1970 nm,[3] and the plasmonic decay rate and quality factor variations shown in Figure 5A, are estimated for a gold nanoparticle of radius r_m ~ 5 nm submerged in water, using the above equations and the following parameters from literature: $\hbar\omega_p \approx 9.02$ eV, $\hbar\Gamma_{abs} \approx 0.071$ eV,[64] $\epsilon_b \approx 1.78$, and $\epsilon_\infty \approx 9.84$.[65]

It has been shown that rather low-quality factors ranging from about 10 to 100 such as those in Figure 5A, accompanied by small effective volumes in the nanometer scale, result in high-quality factor/effective volume ratios that indicate efficient coupling to quantum emitters generally.[61] This is in contrast to conventional diffraction-limited microcavities with comparatively much higher volumes that efficiently couple to emitters thanks to their very high-quality factors.[61] Thus, our

https://doi.org/10.1021/acsanm.1c03522
ACS Appl. Nano Mater. 2022, 5, 3213−3228

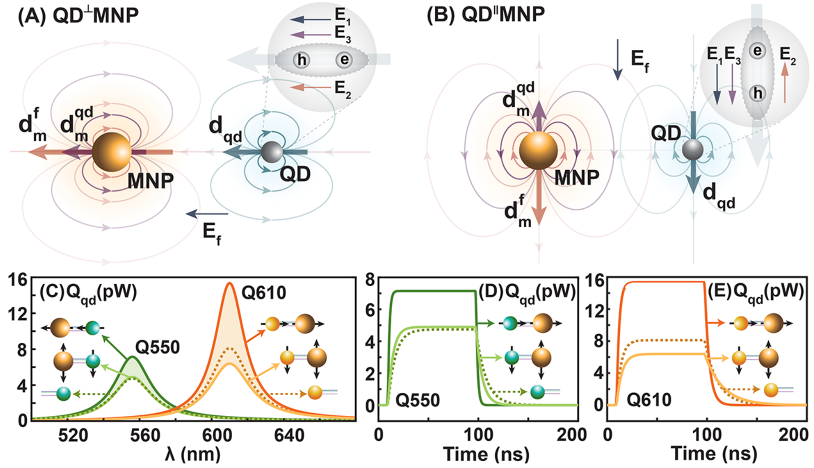

Figure 6. (A,B) Schematic diagrams for the cases where the QD dipoles are perpendicular and parallel to the MNP surface. The exciton formed in the QD experiences three external fields: E_1 (external field E_f screened by the QD material), E_2 (field emanated by the dipole d_m^f formed in the MNP in response to E_f), and E_3 (field emanated by the MNP dipole d_m^{qd} formed in response to the QD dipole d_{qd}). Theoretically generated steady-state and temporal emission spectra for the extreme orientations of Q550-AuNS$_{10}$ and Q610-AuNS$_{10}$ (with the isolated QD plots as references) are shown in panels (C−E). The shaded regions depict where the emission from intermediate orientations would fall. Theoretical formalism and all parameters used are detailed in the Supporting Information.

gold nanoparticle submerged in water is expected to behave as a damped, low-quality factor nanoscale cavity capable of efficiently coupling to emitters, while altering their electromagnetic environments with reasonably high bandwidths.

Using the aforementioned cavity analogy, the density of states $g(\omega)$ of the MNP cavity for a given single mode with half-width $\Delta\omega_c$ and cavity resonance ω_c is estimated as $g(\omega) \sim (2\Delta\omega_c)/\{\pi[4(\omega - \omega_c)^2 + \Delta\omega_c^2]\}$.[62] The qualitatively estimated density of states variation for the dipole mode of the earlier MNP obtained using $\Delta\omega_c \sim \Gamma_1$ and $\omega_c \sim \omega_1$ is depicted in Figure 5B. This results in a Lorentzian-shaped density of states variation suggesting that an MNP seems more likely to accept a photon emitted by a nearly resonant QD due to the high density of states, whereas this ability depletes as the QD becomes off-resonant. In essence, we can interpret the experimentally observed QD decay rate modification as a manifestation of the cavity nature of gold nanoparticles, where the emission is enhanced when the "cavity" is tuned (in Figure 4A for Q550-AuNS$_{10}$) and the emission is suppressed when it is detuned (in Figure 4B for Q610-AuNS$_{10}$), as suggested by eq 1.

In conventional resonant low Q cavities, the rapidity of emitter decay has been reported to increase with the number of emitters.[66] This behavior is marginally mimicked by Q550-AuNS$_{10}$ core−satellite assemblies with average normalized lifetime 6.5 ns/8.4 ns ≈ 0.77 (see Table 1), in comparison to Q550-AuNS$_{10}$ dimers with average normalized lifetime 7.8 ns/9.9 ns ≈ 0.79. Note that the observed difference between the dimer and core−satellite assemblies stems not just from the number of surrounding emitters but also from the (unquantified) increase in the local refractive index of the MNP due to the larger number of DNA strands in the latter case. It has also been reported in the context of conventional cavities that collective emission effects can be appreciably suppressed by increasing the detuning of the cavity from the emitter resonance for multiple emitter assemblies.[66] This is qualitatively mimicked by our experimental observations for Q610-AuNS$_{10}$ Dimer (average normalized lifetime 16.3 ns/12.9 ns ≈ 1.26) and core−satellite assemblies (average normalized lifetime 19.8 ns/12 ns ≈ 1.65). While reporting these qualitative similarities, we also emphasize that MNPs are not expected to ideally mimic conventional, diffraction-limited linear optical cavities. MNPs form feedback dipoles in response to all proximal dipoles,[67,68] which causes emitter−AuNP assemblies to behave as nonlinear systems.

MNP-QD Dimers As Semiclassical Open Quantum Systems. Adopting an alternative viewpoint to account for the aforementioned nonlinearities, the MNP can be modeled using the generalized nonlocal optical response theory (GNOR)[64] and the QD excitons as open quantum systems.

Incorporating GNOR-based nonlocality corrections to the dipolar mode of the Mie expansion, the normalized decay rate for a generic dipolar emitter placed at a small center separation z_0 from a spherical metal nanoparticle can be estimated as

$$\frac{\gamma^{\perp}}{n_b\gamma_0} = \frac{\tau_{ref}}{\tau^{\perp}} \approx \frac{6\,\mathrm{Im}[\alpha_1^{NL}]}{k_b^3 z_0^6} \tag{6a}$$

$$\frac{\gamma^{\parallel}}{n_b\gamma_0} = \frac{\tau_{ref}}{\tau^{\parallel}} \approx \frac{3\,\mathrm{Im}[\alpha_1^{NL}]}{2k_b^3 z_0^6} \tag{6b}$$

where $\gamma^{\perp}$, $\gamma^{\parallel}$, and γ_0 denote the spontaneous emission rates of dipole emitters oriented perpendicular and parallel to the MNP surface and free-space spontaneous decay rate, respectively. The decay rate of the isolated emitter in a medium of refractive index n_b is obtainable as $\gamma_{ref} = n_b\gamma_0$,[69] and τ (with each respective subscript/superscript) denotes the emitter excitation lifetime. See the Supporting Information for details, including the full form of the GNOR-based MNP dipolar polarizability α_1^{NL}. The decay rate γ of a randomly oriented emitter in a hybrid dimer can be estimated as[61]

$$\gamma = (\gamma^{\perp} + 2\gamma^{\parallel})/3 \tag{7}$$

Figure 5C shows that for a generic emitter, the normalized excitation lifetime is expected to increase as the emission frequency moves away from the MNP resonance (and vice versa) as per eqs 6a and 6b in line with our earlier observations and claims. It can also be seen from Figure 5D,E that the PL lifetimes of both Q550 and Q610 are theoretically expected to decrease in response to a gold nanoparticle approaching closer (decreasing z_0) in line with the previous single dimer-based observations in literature.[17] The lifetimes of QDs we reported experimentally (for dimers in Table 1) are averages resulting from the cohort of dimers present in colloidal samples, where the center separations may vary around ~17 nm.

The exciton that forms in the QD is modeled as a coherently illuminated two-level-atom (TLA) coupled to the plasmonic field of the MNP at one of the two extreme orientations (QD transition dipole parallel or perpendicular to the MNP surface as portrayed in Figure 6). The TLA (both in isolation and in the presence of the MNP) is assumed to behave as an open quantum system that undergoes Markovian interactions with the submerging environment. This TLA model, where we equate the excitonic energy gap to the experimentally observed emission spectral peak of a given QD is only expected to approximate the emission behavior, which is the focus of our study. It is not expected to sufficiently capture the phonon-assisted absorption mechanism of the QD which results in an absorption peak that does not overlap with the emission peak (unlike for an ideal TLA). Following the detailed formalism summarized in the Supporting Information, we arrive at the following optical Bloch equations for the density matrix elements of the TLA under the influence of an external electric field and the MNP

$$\dot{\rho}_{\mathrm{ee}} = -\frac{\rho_{\mathrm{ee}}}{\tau^{\angle}} + i\Omega^{r}\tilde{\rho}_{\mathrm{ge}} - i\Omega^{r*}\tilde{\rho}_{\mathrm{eg}} \tag{8a}$$

$$\dot{\rho}_{\mathrm{gg}} = \frac{\rho_{\mathrm{ee}}}{\tau^{\angle}} - i\Omega^{r}\tilde{\rho}_{\mathrm{ge}} + i\Omega^{r*}\tilde{\rho}_{\mathrm{eg}} \tag{8b}$$

$$\dot{\tilde{\rho}}_{\mathrm{eg}} = -[i(\omega_0 - \omega) + 1/T^{\angle}]\tilde{\rho}_{\mathrm{eg}} + i\Omega^{r}(\rho_{\mathrm{gg}} - \rho_{\mathrm{ee}}) \tag{8c}$$

where ρ_{ij} is the ijth density matrix element of the TLA, considering the basis states $\{|g\rangle, |e\rangle\}$, $\rho_{\mathrm{eg}} = \tilde{\rho}_{\mathrm{eg}}e^{-i\omega t}$, $\tilde{\rho}_{\mathrm{ge}} = \tilde{\rho}^{*}_{\mathrm{eg}}$, $\tau^{\angle}$ ($\angle = \{\perp, \|\}$) is the corresponding emitter decay time (lifetime), $T^{\angle}$ is the corresponding dephasing time, ω_0 is the emitter resonance and ω is the angular frequency of the incoming radiation. The effective Rabi frequency in the presence of the MNP (Ω^{r}) is related to the slowly varying positive frequency amplitude ($\tilde{E}^{+}_{\mathrm{qd}}$) of the total field experienced by the QD exciton (E_{qd}) via the QD dipole moment element μ as $\tilde{E}^{+}_{\mathrm{qd}} = \hbar\Omega^{r}/\mu$. E_{qd} is the sum of three field components incident on the QD exciton: E_1 (external field E_f, screened by the QD material), E_2 (field emanated by the dipole formed in the MNP in response to E_{f}), and E_3 (field emanated by the dipole formed in the MNP in response to the QD dipole). A detailed discussion on dipole formation in nanohybrids can be found in ref 68. The total power emitted by the TLA takes the form $Q_{\mathrm{qd}} \sim \hbar\omega_0\rho_{\mathrm{ee}}/\tau^{\angle}$ for the extreme dimer orientations.[67,70] For the isolated QD, $Q_{\mathrm{qd}} \sim \hbar\omega_0[\rho_{\mathrm{ee}}]_{\mathrm{ref}}/\tau_{\mathrm{ref}}$, where $[\rho_{\mathrm{ee}}]_{\mathrm{ref}}$ denotes the isolated QD excited state population (see Supporting Information for details).

The above TLA-based open quantum system formalism is used to theoretically predict the behavior of Q550-AuNS$_{10}$ and Q610-AuNS$_{10}$ dimers in extreme orientations. It is assumed that QDs are isotropic and form dipoles along the external field. It can be seen from Figure 6A that all fields experienced by a QD exciton constructively add in the same direction when the QD dipole is ⊥ to the MNP surface (where all fields form along the axis of the hybrid), always resulting in a stronger field compared to the isolated QD (reference). This results in larger emission from the ⊥ case compared to the reference for both Q550-AuNS$_{10}$ and Q610-AuNS$_{10}$ as observed in Figure 6C (where the darker solid lines for both dimers are larger than the reference). However, in the ∥ orientation (see Figure 6B for the schematic), there can be constructive and destructive interference effects between the field components incident on the QD exciton, resulting in the emission of the dimer being enhanced or suppressed compared to the isolated QD depending on parameter variations. It can be observed from Figure 6C that Q610-AuNS$_{10}$ shows a large steady-state emission enhancement in the ⊥ (axial) orientation compared to Q550-AuNS$_{10}$. This suggests that the larger steady-state emission enhancement we experimentally observed for the Q610-AuNS$_{10}$ colloidal ensemble in Figure 3D, compared to Q550-AuNS$_{10}$ in Figure 3C, is likely to be attributable to the dominant contribution of axial field enhancement.

Temporal PL decay plots theoretically obtained for (single molecules of) both Q550-AuNS$_{10}$ and Q610-AuNS$_{10}$ dimers are depicted in Figure 6D,E. The emission phase of these TLA-based time-domain plots occurs after the electric field input is switched off near 100 ns. Comparison of Q610s steady-state isolated and dimer spectra in Figure 6C to its temporal plots in Figure 6E reveals that the plasmonically enhanced ⊥ case in the former subplot maps to an enhanced temporal decay while the plasmonically suppressed ∥ case maps to a suppressed temporal decay (or an enhanced lifetime, as is also observable from Figure 5). The larger decay rate observed for the ⊥ orientation is expected to be caused by the larger electric field experienced by the QD in the ⊥ orientation compared to the ∥ case as suggested by the Fermi's golden rule in eq 1. Thus, the suppressed QD decay rate experimentally observed for the colloidal Q610-AuNS$_{10}$ dimer ensemble in Figure 4B is likely to be attributable to the dominant contribution of the ∥ components, as suggested by eq 7.

■ OUTLOOK

The formation of highly photostable films of the hybrid assemblies is a preliminary step to incorporate these structures into optical devices. The hybrid assemblies in solution showed good photostability with no noticeable change in their optical properties following illumination with a pulsed laser at 1 mW (10 MHz repetition rate and ~50 ps pulse width) for 30 min. Additionally, the optical properties were monitored over 24 h in solution with no changes detected. Figure S12 shows Q610-AuNS$_{10}$ hybrid dimer assemblies (2 μM, 20 μL) drop-cast on glass followed by evaporation of the solution. The resulting film is luminescent upon exposure to a UV lamp, even after several months. While more rigorous testing is required, these initial results are promising for translation and exploitation of the ensembles in solid devices.

■ CONCLUSION

We combine DNA-based self-assembly methods, optical spectroscopy, and theory to determine the fundamental interactions between plasmonic nanoparticles and quantum dots. Discrete assemblies incorporating quantum dots and gold nanoparticles are synthesized by translation of DNA-based assembly methods to CdSe QDs. The isolation of QDs containing only one strand of DNA per particle allows the formation of QD/AuNP dimers and core−satellite structures in high purity. The tight control of the nanoparticle sizes, stoichiometry, and interparticle separation (via DNA linker length) in the assemblies allows the interrogation of these precise structures using ensemble optical spectroscopy and theory.

A gold nanoparticle immersed in water behaves as a nanoscale damped optical cavity that mimics the qualitative behavior of conventional diffraction-limited optical cavities when modifying the emission characteristics of quantum emitters. We show experimentally and theoretically that the detuning between a metal nanoparticle and an emitter can be effectively used for the regulation (enhancement/suppression) of spontaneous emission from quantum dots. The observed lowering of the QD emission rate (by a factor of up to 1.7) gives a mechanism for greater control over the QD emission lifetime by a plasmonic nanoparticle than previously appreciated.

We show that the luminescence of QDs in the presence of a gold nanoparticle is enhanced. The steady-state emission is increased for the off-resonant dimer compared to the closely resonant dimer. Using an open quantum system-based analysis on extreme metal-QD dimer orientations, this is attributed to the dominance of axial enhancement of the electric field, and consequently the steady-state QD spectra.

The enhanced photoluminescence intensity and lifetime lengthening are promising for use of these hybrids in LEDs and solar harvesting/photovoltaics. In addition, the exploitation of DNA within the nanostructures opens up the future possibility of achieving dynamic control of exciton−plasmon systems, paving the way for use of the assemblies in optoelectronic applications requiring exciton-based switching.

■ EXPERIMENTAL SECTION

Materials. Cadmium oxide (CdO) (99%), octadecene (ODE) (technical grade, 90%), oleylamine (technical grade, 70%), trioctylphosphine (90%), oleic acid (technical grade, 90%), octane thiol (≥98.5%), tetradecylphosphonic acid, selenium powder (Se) (99.00%), sulfur (≥99.99%), sodium borohydride ($NaBH_4$) (≥99%), gold(III) chloride trihydrate (≥99.9%), tannic acid, trisodium citrate dihydrate (≥98.5%), bis(*p*-sulfonatophenyl)phenylphosphine (BSPP) (97%), potassium carbonate, phosphonoacetic acid (98%), agarose (type I, low EEO), boric acid, Tris base, chloroform (high-pressure liquid chromatography (HPLC) grade), EDTA, and Ficoll 400 were purchased from Sigma-Aldrich. CTAB (98%) was purchased from Ajax Finechem; acetone (analytical reagent (AR) grade) and methanol (AR grade) were purchased from Merck. Thiolated ethylene glycol HS-C_{11}-$(EG)_6$-OCH_2-COOH was purchased from Prochimia Surface (Poland). Tetramethylammonium hydroxide (TMAOH) (25% w/w in methanol) was purchased from Alfa Aesar.

PAGE-purified trithiolated DNA sequences were purchased from Fidelity Systems, Inc. (U.S.A.). The sequences of DNA used for DNA-based self-assembly are given below.

A1: 5′-trithiol-TTTTCTCACTAAGATCGATAGAGCGATTGTGATATTTCAAGCGGTACTCCAGCTCTAGGTAGCTCCCTTTCCAATCAGCTTATGTGAGCGCCTGCCCATG-3′

A1-comp: 5′-trithiol-TTTCATGGGCAGGCGCTCACATAAGCTGATTGGAAAGGGAGCTACCTAGAGCTGGAGTACCGCTTGAAATATCACAATCGCTCTATCGATCTTAGTGAGA-3′

B1: 5′-trithiol-TATACCTGACCTCGGGACTTGACTGATTGT-3′

B1-comp: 5′-trithiol-ACAATCAGTCAAGTCCCGAGGTCAGGTATA-3′

L1: 5′-GCTGACTCGCTACTCTTTTTTTTTTTTTTTTTTTTTTTTTTTTTTTTTTTTTTTTTTTTTTTTTTTTTTTTTTTTTTGCATGCAGATACAATCAGTCAAGTC-3′

L1-comp: 5′-GACTTGACTGATTGTATCTGCATGCTTTTTTTTTTTTTTTTTTTTTTTTTTTTTTTTTTTTTTTTTTTTTTTTTTTTTTTTTTGAGTAGCGAGTCAGC-3′

L2: 5′-AGCACACAAGAGCTGTTTTTTTTTTTTTTTTTTTTTTTTTTTTTTTTTTTTTTTTTTTTTTTTTTTTTTTTTTTTTTTAGCAGATACATATACCTGACCTCGG-3′

L2-comp: 5′-CCGAGGTCAGGTATATGTATCTGCTTTTTTTTTTTTTTTTTTTTTTTTTTTTTTTTTTTTTTTTTTTTTTTTTTTTTTTTTTTTCAGCTCTTGTGTGCT-3′

All chemicals were used as received without further purification. Ultrapure water from a Milli-Q system with resistivity >18 MΩ was used for all aqueous solutions.

Synthesis. *Gold Nanoparticles.* Gold nanospheres were synthesized according to the method described by Piella et al.[47] Different aspect ratios of gold nanorods were synthesized using the method reported by Nikoobakht and El-Sayed.[48]

Quantum Dots. Quantum dot nanocrystals were synthesized according to the published protocol of Boldt et al.[49]

Ligand Exchange of Nanoparticles. Quantum dots were transferred from the organic to aqueous phase by ligand exchange. For this, phosphonoacetic acid (PsAA) (0.1 M, 5 mL) solution was prepared in methanol and added to a dispersion of the QDs in chloroform (13 μM, 1.00 mL). The pH of the PsAA solution was maintained using TMAOH (tetramethylaluminum hydroxide, 25% solution in methanol). The QD dispersion in chloroform was added, and then the dispersion was sonicated for 1−2 min. Water was added and the QDs migrated to the aqueous layer following sonication, leaving a colorless organic layer. The aqueous layer containing the QDs was collected and washed twice by precipitation via the addition of acetone (∼5−10 mL). The precipitate was centrifuged and the pellet was redispersed in water to remove excess PsAA.

Colloidal gold nanoparticles with citrate ligands with a diameter of 10 nm were mixed overnight with BSPP (200.0 μL, 90.0 mM). These were then purified by centrifugation at 13 400 rpm for 50 min. The supernatant was removed and the pellet redispersed in BSPP buffer and washed three more times to achieve colloidally stable gold nanoparticles. After the final washing, the pellet was collected and redispersed in a known volume of BSPP to achieve a final concentration of nanoparticles (2−5 μM).

NP-DNA Functionalization. *QDs-Short (30 bp) DNA Conjugation.* Thiolated short DNA (100.0 μM) (0.5, 1.0, 2.0, 3.0, 4.0, and 5.0 μL) was mixed with the equimolar concentration of nonfunctionalized lengthening DNA strands (100 bp) which was then left to incubate overnight. The DNA solution was then added to the highly concentrated quantum dot solution (25.0 μM, 5 μL) in the presence of BSPP (90.0 mM, 1.0 μL) and NaCl (1 M, 1 mL). The samples were incubated overnight before running on the gel for purification.

QDs-Long (100 bp) DNA Conjugation. Thiolated DNA (100.0 μM) (0.5, 1.0, 2.0, 3.0, 4.0, and 5.0 μL) was added to highly concentrated quantum dot solution (25.0 μM, 5 μL) in the presence of BSPP (90.0 mM, 1.0 μL) and NaCl (1 M, 1 mL). The samples were incubated overnight before running on the gel for purification.

AuNP-Short (30 bp) DNA Conjugation. Short (30 bp) thiolated DNA (0.5, 1.0, 2.0, 3.0, 4.0, and 5.0 μL of 100.0 μM) were mixed with an equimolar concentration of nonfunctionalized lengthening DNA strands (100 bp) and the dispersion left to incubate overnight. The DNA solution was then added to the highly concentrated gold nanoparticle solution (2−5 μM, 5 μL) in the presence of BSPP (90.0 mM, 1.0 μL) and NaCl (1 M, 1 mL). The samples were incubated overnight before running on the gel for purification.

AuNP-Long (100 bp) DNA Conjugation. The thiol-functionalized DNA (0.1, 1.0, 3.0, and 10.0 μL of 100.0 μM) were separately mixed with the highly concentrated dispersion of gold nanoparticles (AuNP) (2−5 μM, 5.0 μL) in the presence of salt (NaCl) (1.0 M, 1 mL) and BSPP (90.0 mM, 1.0 μL). The samples were left overnight for incubation.

Purification of NP-DNA Conjugates. Prior to electrophoresis (15 min), mPEG (∼100 000−500 000 molar excess with respect to the AuNP concentration, 1.0 μL) was added to the Au-DNA samples and HS-C_{11}-$(EG)_6$-OCH_2-COOH (340× excess with respect to the QDs concentration, 1.0 μL) to the QD-DNA samples. Before loading the samples on the gel, Ficoll solution (20%, 4.0 μL) was added as a loading buffer to increase the density of samples. The nanoparticle−DNA conjugate mixtures containing different concentrations of DNA were loaded on the agarose gel (2.7% for AuNPs, 4.1% for Q550, 3.8% for Q570, 3.4% for Q610, and 3.2% for Q650). For the electrophoresis, the voltage was set to 80 V for 35−45 min. The same procedure was performed for all Au and QD particles for both pairs of complementary DNA strands. An electroelution procedure was used to extract AuNP−DNA conjugates from the gel and the extracted solution was concentrated via centrifugation before hybridization. For the extraction of QD-DNA conjugates, gel bands were cut and soaked in 0.5× TBE buffer overnight. The resulting dispersion was then concentrated by evaporating the solution under N_2 stream.

For COSA assemblies, the central AuNP was mixed with a higher DNA concentration (10-fold excess) to fully allow the DNA coverage around AuNP. The samples were left overnight for DNA conjugation and were then run on 1% (w/v) of the agarose gel for purifying it from the unbound DNA strands.

For the preparation of gel, agarose powder was mixed with 0.5x TBE buffer to give the desired concentration of gel. The mixture was heated in the microwave oven (800 W) for 2 min to dissolve the gel. The gel was cooled to ∼60−70 °C and poured into the electrophoresis tray. When the gel was fully solidified, the comb was removed. The gel was immersed in 0.5X TBE buffer. The sample was loaded into the wells, and electrophoresis was carried out at 80 V for 35 min.

Self-Assembly and Purification. After achieving purified samples containing the desired number of DNA strands per particle, AuNS and QDs with one DNA and one complementary DNA strand/particle respectively were mixed together in the presence of optimized salt concentration (1 M, 1.0 μL) to form the hybrid dimer assembly. Hybrid COSA assemblies were formed after mixing the central fully DNA functionalized AuNP cores with one complementary DNA containing QD satellite particles in the presence of salt (2 M, 1.0 μL).

The assemblies were run in the second gel electrophoresis step on a dilute gel (1−2.5%) to purify the dimer assembly from the unconjugated Au and QD particles and the satellite bearing core nanoparticles from the unbound satellites. The low mobility rate of dimers and core−satellites assemblies compared to single unconjugated nanoparticles was responsible for separate bands while running on the agarose gel. Therefore, the relative mobility rate forms the basis of purification of an assembly from the unconjugated nanoparticles. The band containing the purified structures of interest was cut from the gel, and the assembly samples were extracted separately from each band by the electroelution procedure. The assembly solution was then concentrated upon centrifugation.

The assembly yields are estimated from the resultant gels. The yield of particles functionalized with one or two DNA strands is dependent upon the DNA concentration. The cross-section of the agarose gel for a typical functionalization used here for both Au and QDs is shown in Figure S3. Taking intensity as proportional to the number of particles in the band, the relative yield of particles attached to a given number of DNA strands per particle is able to be measured. For example, the gel image in Figure S3A shows 30% monomer ($AuNS_{10}$ with no DNA), 55% $AuNS_{10}$ containing a single DNA strand, 10% $AuNS_{10}$ with two DNA strands attached and 5% for 3DNA strands per $AuNS_{10}$ particle. Figure S3B indicates the yield of 35%, 40%, and 25% for Q550 with no DNA, 1DNA, and 2DNA per Q550 particle, respectively. Similarly, under the conditions used the yield of the assembled hybrid dimers from the single DNA functionalized nanoparticles is also calculated from the intensity distribution, that is, 25% for Q550-$AuNS_{10}$, 40% for 1DNA/$AuNS_{10}$, and 35% for 1DNA/Q550 as shown in Figure S3C. We note that here a relatively low concentration of DNA is added to the samples to avoid forming particles with higher numbers of DNA strands, allowing separation of the resultant conjugated particles and optimization of the yield of particles containing one DNA strand per particle.

Calculating Concentrations for Hybrid Assemblies. We used inductively coupled plasma mass spectrometry (ICP-MS) to determine the concentrations of QDs in the hybrid assembly. An eight-point calibration curve was constructed using the known standard solutions of various concentrations. The correlation curves showed an r_2 value of 0.99. The concentration of the QDs was calculated using the isotopes of Cd(111), Cd(112), Se (78), Se (82), Zn(66), Zn(68), and Au(197).

Sample Preparation. Samples for electron microscopy were prepared by depositing 10 μL of the purified assembly on an ultrathin TEM grid which was then soaked in a 1:1 mixture of water and ethanol for 10−15 min. The substrate was then rinsed with absolute ethanol and allowed to dry. Quartz cuvettes of 3 mm path length were used for all photophysical measurements. The cuvette was precleaned by soaking in a nitric acid bath overnight and then washed with copious amounts of water.

Instrumentation. TEM was performed on FEI Tecnai T20 Twin LaB6. Scanning electron microscopy was done on FEI Magellan 400 FEG SEM.

ICP-MS measurements were carried out using a PerkinElmer Nexion 350 ICP-MS instrument.

UV−visible spectra were collected using an Agilent Cary 60 UV−vis Spectrophotometer.

The luminescence spectra of the samples were recorded on a Cary Eclipse Fluorescence Spectrophotometer. For measuring the photoluminescence signal, the optical density of the samples was kept below 0.1 to avoid the inner filter effect.

Photophysical Measurements. The excitation and emission parameters used for the steady-state PL measurements were as follows: excitation wavelength = 425 nm, excitation slit = 5 nm, emission slit = 5 nm, scan rate = 600 nm/min and integration time = 0.1 s.

Time Correlated Single Photon Counting. The fluorescence lifetime decays of both the reference and the assembled quantum dots were measured via a home-built time-resolved single-photon counting (TCSPC) setup. Excitation was provided by a picosecond pulsed supercontinuum laser (Fianium, SC 400-4-pp) with the emission wavelength of 425 nm, selected using a 10 nm bandpass filter (laser power = 1 mW). The emission signal was collected at right angles to the excitation beam which was then directed toward the Multichannel plate detector. Photon emissions were recorded by a photon counting module (PicoHarp 300, Picoquant). The instrument response function (IRF) was measured by using a scattering solution of milk powder in water to be 0.6 ns. The TCSPC data was collected at the 5 MHz frequency and 32 ps time intervals.

Data Analysis. The time-resolved emission decays were fit with convolution with the IRF to a series of exponential functions until a good fit was obtained as judged by the reduced χ^2 value and the randomness of residuals. The fits were performed in custom-written routines in Igor Pro 6.3 software.

■ ASSOCIATED CONTENT

Supporting Information

The Supporting Information is available free of charge at https://pubs.acs.org/doi/10.1021/acsanm.1c03522.

> Electron microscopy images of colloids, steady state spectra of all QDs and gold nanoparticles, wide-field images of assemblies, quantification of number of satellites in core−satellite assemblies, lifetime and steady-state data for assemblies with 100 bp DNA linkers and incorporating Q570 and Q650, along with tabulations of fit data (PDF)

■ AUTHOR INFORMATION

Corresponding Authors

Jared H. Cole − *ARC Centre of Excellence in Exciton Science and Chemical and Quantum Physics, School of Science, RMIT University, Melbourne 3001, Australia;*
Email: jared.cole@rmit.edu.au

Alison M. Funston − *ARC Centre of Excellence in Exciton Science and School of Chemistry, Monash University, Clayton, Victoria 3800, Australia;* orcid.org/0000-0002-4320-6434; Email: alison.funston@monash.edu

Authors

Anum Nisar − *ARC Centre of Excellence in Exciton Science and School of Chemistry, Monash University, Clayton, Victoria 3800, Australia*

Harini Hapuarachchi − *ARC Centre of Excellence in Exciton Science and Chemical and Quantum Physics, School of Science, RMIT University, Melbourne 3001, Australia*

Laurent Lermusiaux − *ARC Centre of Excellence in Exciton Science and School of Chemistry, Monash University, Clayton, Victoria 3800, Australia;* Present Address: Université de Lyon, CNRS, École Normale Supérieure de Lyon, Laboratoire de Chimie UMR 5182, 46 allée d'Italie, F-69007 Lyon, France

Complete contact information is available at: https://pubs.acs.org/10.1021/acsanm.1c03522

Notes

The authors declare no competing financial interest.

■ ACKNOWLEDGMENTS

This work was undertaken within the ARC Centre of Excellence in Exciton Science, supported by the Australian Research Council (ARC) Grant CE170100026. The authors acknowledge the use of instruments and scientific and technical assistance at the Monash Centre for Electron Microscopy, a Node of Microscopy Australia. Computational resources were provided by the National Computational Infrastructure (NCI) at the Australian National University. H.H. gratefully acknowledges Roslyn Forecast and Francesco Campaioli for insightful discussions.

■ REFERENCES

(1) Costa-Fernández, J. M.; Pereiro, R.; Sanz-Medel, A. The use of luminescent quantum dots for optical sensing. *Trends Analyt. Chem.* **2006**, *25*, 207−218.

(2) Baskoutas, S.; Terzis, A. F. Size-dependent band gap of colloidal quantum dots. *J. Appl. Phys.* **2006**, *99*, 013708.

(3) Kim, N.-Y.; Hong, S.-H.; Kang, J.-W.; Myoung, N.; Yim, S.-Y.; Jung, S.; Lee, K.; Tu, C. W.; Park, S.-J. Localized surface plasmon-enhanced green quantum dot light-emitting diodes using gold nanoparticles. *RSC Adv.* **2015**, *5*, 19624−19629.

(4) Pan, J.; Chen, J.; Zhao, D.; Huang, Q.; Khan, Q.; Liu, X.; Tao, Z.; Zhang, Z.; Lei, W. Surface plasmon-enhanced quantum dot light-emitting diodes by incorporating gold nanoparticles. *Opt. Express* **2016**, *24*, A33−A43.

(5) Manuel, A. P.; Kirkey, A.; Mahdi, N.; Shankar, K. Plexcitonics-fundamental principles and optoelectronic applications. *J. Mater. Chem. C* **2019**, *7*, 1821−1853.

(6) Hapuarachchi, H.; Mallawaarachchi, S.; Hattori, H. T.; Zhu, W.; Premaratne, M. Optoelectronic figure of merit of a metal nanoparticle—quantum dot (MNP-QD) hybrid molecule for assessing its suitability for sensing applications. *J. Phys.: Condens. Matter* **2018**, *30*, 054006.

(7) Liu, Y.; Dai, X.; Mallawaarachchi, S.; Hapuarachchi, H.; Shi, Q.; Dong, D.; Thang, S. H.; Premaratne, M.; Cheng, W. Poly (n-isopropylacrylamide) capped plasmonic nanoparticles as resonance intensity-based temperature sensors with linear correlation. *J. Mater. Chem. C* **2017**, *5*, 10926−10932.

(8) Hapuarachchi, H.; Premaratne, M.; Bao, Q.; Cheng, W.; Gunapala, S. D.; Agrawal, G. P. Cavity QED analysis of an exciton-plasmon hybrid molecule via the generalized nonlocal optical response method. *Phys. Rev. B* **2017**, *95*, 245419.

(9) Gettapola, K.; Hapuarachchi, H.; Stockman, M. I.; Premaratne, M. Control of quantum emitter-plasmon strong coupling and energy transport with external electrostatic fields. *J. Phys.: Condens. Matter* **2020**, *32*, 125301.

(10) Hapuarachchi, H.; Gunapala, S. D.; Bao, Q.; Stockman, M. I.; Premaratne, M. Exciton behavior under the influence of metal nanoparticle near fields: Significance of nonlocal effects. *Phys. Rev. B* **2018**, *98*, 115430.

(11) Sajanlal, P. R.; Sreeprasad, T. S.; Samal, A. K.; Pradeep, T. Anisotropic nanomaterials: structure, growth, assembly, and functions. *Nano Rev.* **2011**, *2*, 5883.

(12) Kim, K.-S.; Zakia, M.; Yoon, J.; Yoo, S. I. Metal-enhanced fluorescence in polymer composite films with Au@ Ag@ SiO 2 nanoparticles and InP@ ZnS quantum dots. *RSC Adv.* **2019**, *9*, 224−233.

(13) LeBlanc, S. J.; McClanahan, M. R.; Jones, M.; Moyer, P. J. Enhancement of multiphoton emission from single CdSe quantum dots coupled to gold films. *Nano Lett.* **2013**, *13*, 1662−1669.

(14) Kulakovich, O.; Strekal, N.; Yaroshevich, A.; Maskevich, S.; Gaponenko, S.; Nabiev, I.; Woggon, U.; Artemyev, M. Enhanced luminescence of CdSe quantum dots on gold colloids. *Nano Lett.* **2002**, *2*, 1449−1452.

(15) Chaikin, Y.; Kedem, O.; Raz, J.; Vaskevich, A.; Rubinstein, I. Stabilization of metal nanoparticle films on glass surfaces using ultrathin silica coating. *Anal. Chem.* **2013**, *85*, 10022−10027.

(16) Jensen, T. R.; Malinsky, M. D.; Haynes, C. L.; Van Duyne, R. P. Nanosphere lithography: tunable localized surface plasmon resonance spectra of silver nanoparticles. *J. Phys. Chem. B* **2000**, *104*, 10549−10556.

(17) Ratchford, D.; Shafiei, F.; Kim, S.; Gray, S. K.; Li, X. Manipulating coupling between a single semiconductor quantum dot and single gold nanoparticle. *Nano Lett.* **2011**, *11*, 1049−1054.

(18) Sen, T.; Sadhu, S.; Patra, A. Surface energy transfer from rhodamine 6G to gold nanoparticles: A spectroscopic ruler. *Appl. Phys. Lett.* **2007**, *91*, 043104.

(19) Wargnier, R.; Baranov, A. V.; Maslov, V. G.; Stsiapura, V.; Artemyev, M.; Pluot, M.; Sukhanova, A.; Nabiev, I. Energy transfer in aqueous solutions of oppositely charged CdSe/ZnS core/shell quantum dots and in quantum dot- nanogold assemblies. *Nano Lett.* **2004**, *4*, 451−457.

(20) Ofir, Y.; Samanta, B.; Rotello, V. M. Polymer and biopolymer mediated self-assembly of gold nanoparticles. *Chem. Soc. Rev.* **2008**, *37*, 1814−1825.

(21) Quintiliani, M.; Bassetti, M.; Pasquini, C.; Battocchio, C.; Rossi, M.; Mura, F.; Matassa, R.; Fontana, L.; Russo, M. V.; Fratoddi, I. Network assembly of gold nanoparticles linked through fluorenyl dithiol bridges. *J. Mater. Chem. C* **2014**, *2*, 2517−2527.

(22) Lin, G.; Chee, S. W.; Raj, S.; Král, P.; Mirsaidov, U. Linker-mediated self-assembly dynamics of charged nanoparticles. *ACS Nano* **2016**, *10*, 7443−7450.

(23) Li, H.; Carter, J. D.; LaBean, T. H. Nanofabrication by DNA self-assembly. *Mater. Today* **2009**, *12*, 24−32.

(24) Schreiber, R.; Do, J.; Roller, E.-M.; Zhang, T.; Schüller, V. J.; Nickels, P. C.; Feldmann, J.; Liedl, T. Hierarchical assembly of metal nanoparticles, quantum dots and organic dyes using DNA origami scaffolds. *Nat. Nanotechnol.* **2014**, *9*, 74−78.

(25) Wang, R.; Nuckolls, C.; Wind, S. J. Assembly of heterogeneous functional nanomaterials on DNA origami scaffolds. *Angew. Chem., Int. Ed.* **2012**, *51*, 11325−11327.

(26) Zhang, T.; Liedl, T. DNA-Based Assembly of Quantum Dots into Dimers and Helices. *Nanomaterials* **2019**, *9*, 339.

(27) Liu, N.; Liedl, T. DNA-assembled advanced plasmonic architectures. *Chem. Rev.* **2018**, *118*, 3032−3053.

(28) Guerrini, L.; McKenzie, F.; Wark, A. W.; Faulds, K.; Graham, D. Tuning the interparticle distance in nanoparticle assemblies in suspension via DNA-triplex formation: correlation between plasmonic

and surface-enhanced Raman scattering responses. *Chem. Sci.* **2012**, *3*, 2262−2269.

(29) Alivisatos, A. P.; Johnsson, K. P.; Peng, X.; Wilson, T. E.; Loweth, C. J.; Bruchez, M. P.; Schultz, P. G. Organization of'nanocrystal molecules' using DNA. *Nature* **1996**, *382*, 609−611.

(30) Fu, A.; Micheel, C. M.; Cha, J.; Chang, H.; Yang, H.; Alivisatos, A. P. Discrete nanostructures of quantum dots/Au with DNA. *J. Am. Chem. Soc.* **2004**, *126*, 10832−10833.

(31) Tikhomirov, G.; Hoogland, S.; Lee, P.; Fischer, A.; Sargent, E. H.; Kelley, S. O. DNA-based programming of quantum dot valency, self-assembly and luminescence. *Nat. Nanotechnol.* **2011**, *6*, 485.

(32) Lermusiaux, L.; Nisar, A.; Funston, A. M. Flexible synthesis of high-purity plasmonic assemblies. *Nano Res.* **2021**, *14*, 635−645.

(33) Vaishnav, J. K.; Mukherjee, T. K. Long-range resonance coupling-induced surface energy transfer from CdTe quantum dot to plasmonic nanoparticle. *J. Phys. Chem. C* **2018**, *122*, 28324−28336.

(34) Pons, T.; Medintz, I. L.; Sapsford, K. E.; Higashiya, S.; Grimes, A. F.; English, D. S.; Mattoussi, H. On the quenching of semiconductor quantum dot photoluminescence by proximal gold nanoparticles. *Nano Lett.* **2007**, *7*, 3157−3164.

(35) Tripathi, L.; Praveena, M.; Valson, P.; Basu, J. Long range emission enhancement and anisotropy in coupled quantum dots induced by aligned gold nanoantenna. *Appl. Phys. Lett.* **2014**, *105*, 163106.

(36) Tripathi, L.; Praveena, M.; Basu, J. Plasmonic tuning of photoluminescence from semiconducting quantum dot assemblies. *Plasmonics* **2013**, *8*, 657−664.

(37) Nikoobakht, B.; Burda, C.; Braun, M.; Hun, M.; El-Sayed, M. A. The Quenching of CdSe Quantum Dots Photoluminescence by Gold Nanoparticles in Solution. *Photochem. Photobiol.* **2002**, *75*, 591−597.

(38) Huang, Q.; Chen, J.; Zhao, J.; Pan, J.; Lei, W.; Zhang, Z. Enhanced photoluminescence property for quantum dot-gold nanoparticle hybrid. *Nanoscale Res. Lett.* **2015**, *10*, 1−6.

(39) Liu, N.; Prall, B. S.; Klimov, V. I. Hybrid gold/silica/nanocrystal-quantum-dot superstructures: synthesis and analysis of semiconductor- metal interactions. *J. Am. Chem. Soc.* **2006**, *128*, 15362−15363.

(40) Inoue, A.; Fujii, M.; Sugimoto, H.; Imakita, K. Surface plasmon-enhanced luminescence of silicon quantum dots in gold nanoparticle composites. *J. Phys. Chem. C* **2015**, *119*, 25108−25113.

(41) Kormilina, T.; Stepanidenko, E.; Cherevkov, S.; Dubavik, A.; Baranov, M.; Fedorov, A.; Baranov, A.; Gun'Ko, Y.; Ushakova, E. A highly luminescent porous metamaterial based on a mixture of gold and alloyed semiconductor nanoparticles. *J. Mater. Chem. C* **2018**, *6*, 5278−5285.

(42) Ribeiro, T.; Prazeres, T.; Moffitt, M.; Farinha, J. Enhanced photoluminescence from micellar assemblies of cadmium sulfide quantum dots and gold nanoparticles. *J. Phys. Chem. C* **2013**, *117*, 3122−3133.

(43) Nepal, D.; Drummy, L. F.; Biswas, S.; Park, K.; Vaia, R. A. Large scale solution assembly of quantum dot-gold nanorod architectures with plasmon enhanced fluorescence. *ACS Nano* **2013**, *7*, 9064−9074.

(44) Hsieh, Y.-P.; Liang, C.-T.; Chen, Y.-F.; Lai, C.-W.; Chou, P.-T. Mechanism of giant enhancement of light emission from Au/CdSe nanocomposites. *Nanotechnology* **2007**, *18*, 415707.

(45) Song, J.-H.; Atay, T.; Shi, S.; Urabe, H.; Nurmikko, A. V. Large enhancement of fluorescence efficiency from CdSe/ZnS quantum dots induced by resonant coupling to spatially controlled surface plasmons. *Nano Lett.* **2005**, *5*, 1557−1561.

(46) Li, J.; Krasavin, A. V.; Webster, L.; Segovia, P.; Zayats, A. V.; Richards, D. Spectral variation of fluorescence lifetime near single metal nanoparticles. *Sci. Rep.* **2016**, *6*, 1−10.

(47) Piella, J.; Bastús, N. G.; Puntes, V. Size-Controlled Synthesis of Sub-10-nanometer Citrate-Stabilized Gold Nanoparticles and Related Optical Properties. *Chem. Mater.* **2016**, *28*, 1066−1075.

(48) Nikoobakht, B.; El-Sayed, M. A. Preparation and growth mechanism of gold nanorods (NRs) using seed-mediated growth method. *Chem. Mater.* **2003**, *15*, 1957−1962.

(49) Boldt, K.; Kirkwood, N.; Beane, G. A.; Mulvaney, P. Synthesis of Highly Luminescent and Photo-Stable, Graded Shell CdSe/Cd x Zn1-x S Nanoparticles by In Situ Alloying. *Chem. Mater.* **2013**, *25*, 4731−4738.

(50) Busson, M. P.; Rolly, B.; Stout, B.; Bonod, N.; Larquet, E.; Polman, A.; Bidault, S. Optical and topological characterization of gold nanoparticle dimers linked by a single DNA double strand. *Nano Lett.* **2011**, *11*, 5060−5065.

(51) Busson, M. P.; Rolly, B.; Stout, B.; Bonod, N.; Larquet, E.; Polman, A.; Bidault, S. Optical and topological characterization of gold nanoparticle dimers linked by a single DNA double strand. *Nano Lett.* **2011**, *11*, 5060−5065.

(52) Yao, H.; Yi, C.; Tzang, C.-H.; Zhu, J.; Yang, M. DNA-directed self-assembly of gold nanoparticles into binary and ternary nanostructures. *Nanotechnology* **2007**, *18*, 015102.

(53) Lermusiaux, L.; Funston, A. M. Plasmonic isomers via DNA-based self-assembly of gold nanoparticles. *Nanoscale* **2018**, *10*, 19557−19567.

(54) Chen, Z.; Lan, X.; Chiu, Y.-C.; Lu, X.; Ni, W.; Gao, H.; Wang, Q. Strong chiroptical activities in gold nanorod dimers assembled using DNA origami templates. *ACS Photonics* **2015**, *2*, 392−397.

(55) Park, S.-J.; Lazarides, A. A.; Storhoff, J. J.; Pesce, L.; Mirkin, C. A. The structural characterization of oligonucleotide-modified gold nanoparticle networks formed by DNA hybridization. *J. Phys. Chem. B* **2004**, *108*, 12375−12380.

(56) Kulakovich, O.; Strekal, N.; Yaroshevich, A.; Maskevich, S.; Gaponenko, S.; Nabiev, I.; Woggon, U.; Artemyev, M. Enhanced luminescence of CdSe quantum dots on gold colloids. *Nano Lett.* **2002**, *2*, 1449−1452.

(57) Li, X.; Kao, F.-J.; Chuang, C.-C.; He, S. Enhancing fluorescence of quantum dots by silica-coated gold nanorods under one-and two-photon excitation. *Opt. Express* **2010**, *18*, 11335−11346.

(58) Cohen-Hoshen, E.; Bryant, G. W.; Pinkas, I.; Sperling, J.; Bar-Joseph, I. Exciton-plasmon interactions in quantum dot-gold nanoparticle structures. *Nano Lett.* **2012**, *12*, 4260−4264.

(59) Nepal, D.; Drummy, L. F.; Biswas, S.; Park, K.; Vaia, R. A. Large scale solution assembly of quantum dot-gold nanorod architectures with plasmon enhanced fluorescence. *ACS Nano* **2013**, *7*, 9064−9074.

(60) Vaishnav, J. K.; Mukherjee, T. K. Long-range resonance coupling-induced surface energy transfer from CdTe quantum dot to plasmonic nanoparticle. *J. Phys. Chem. C* **2018**, *122*, 28324−28336.

(61) Colas des Francs, G.; Derom, S.; Vincent, R.; Bouhelier, A.; Dereux, A. Mie plasmons: modes volumes, quality factors, and coupling strengths (purcell factor) to a dipolar emitter. *Int. J. Opt.* **2012**, *2012*, 1.

(62) Fox, M. *Quantum Optics: An Introduction*; OUP Oxford, 2006; Vol. *15*.

(63) Premaratne, M.; Agrawal, G. P. *Theoretical Foundations of Nanoscale Quantum Devices*; Cambridge University Press, 2021; Chapter 1.

(64) Raza, S.; Bozhevolnyi, S. I.; Wubs, M.; Mortensen, N. A. Nonlocal optical response in metallic nanostructures. *J. Phys.: Condens. Matter* **2015**, *27*, 183204.

(65) Kolwas, K.; Derkachova, A. Plasmonic abilities of gold and silver spherical nanoantennas in terms of size dependent multipolar resonance frequencies and plasmon damping rates. *Opto-Electron. Rev.* **2010**, *18*, 429−437.

(66) Seke, J.; Rattay, F. N-atom spontaneous emission in a detuned damped cavity. *J. Opt. Soc. Am. B* **1987**, *4*, 380−386.

(67) Artuso, R. D. *The Optical Response of Strongly Coupled Quantum Dot-Metal Nanoparticle Hybrid Systems*. Ph.D. Thesis, University of Maryland, College Park, Maryland, United States, 2012.

(68) Hapuarachchi, H.; Cole, J. H. Influence of a planar metal nanoparticle assembly on the optical response of a quantum emitter. *Phys. Rev. Res.* **2020**, *2*, 043092.

(69) Duan, C.-K.; Reid, M. F. Dependence of the spontaneous emission rates of emitters on the refractive index of the surrounding media. *J. Alloys Compd.* **2006**, *418*, 213−216.

(70) Wrigge, G. *Coherent and incoherent light scattering in the resonance fluorescence of a single molecule*. Ph.D. Thesis, ETH Zurich, Zurich, Switzerland, 2008.

Recommended by ACS

Controlled Organization of Inorganic Materials Using Biological Molecules for Activating Therapeutic Functionalities

Morgan Chandler, Kirill A. Afonin, *et al.*

AUGUST 17, 2021
ACS APPLIED MATERIALS & INTERFACES
READ

Metal-Enhanced Fluorescence from Quantum Dot-Coupled Gold Nanoparticles

Andrew K. Tobias and Marcus Jones

DECEMBER 21, 2018
THE JOURNAL OF PHYSICAL CHEMISTRY C
READ

Single CdSe Quantum Dots Positioned in Nanostructured Heterogeneous Templates: Implications for High-Precision Nanoassembly

Gang Cheng, Weihua Zhang, *et al.*

APRIL 06, 2022
ACS APPLIED NANO MATERIALS
READ

Excitation Wavelength-Dependent Photoluminescence Decay of Hybrid Gold/Quantum Dot Nanostructures

Terianna J. Wax, Jing Zhao, *et al.*

OCTOBER 25, 2018
ACS OMEGA
READ

Get More Suggestions >